When Does Multipath Improve Imaging Resolution?

Nishant Mehrotra, Student Member, IEEE, and Ashutosh Sabharwal, Fellow, IEEE

Abstract—In this paper, we characterize resolution limits for imaging in electromagnetic spectrum where multipath is commonly encountered, e.g., spectrum often used for wireless communication. We analyze a passive system configuration with an aperture of fixed spatial extent sampling fields backscattered from an imaging scene consisting of both line-of-sight (LOS) and non-line-of-sight (NLOS) paths. We characterize the resolution limits using the degrees of freedom (DoF) metric. We make progress towards answering the question: when does multipath offer gains in imaging resolution over LOS-only propagation? Prior theoretical and empirical analysis offer seemingly contradictory answers to this question. On the one hand, prior theoretical analysis suggests that multipath does not improve resolution beyond LOS-only propagation. However, numerical simulations of multipath-exploiting imaging suggest otherwise. We show that the prior results correspond to two extreme operational regimes, under which multipath is equivalent to either LOS-only or NLOS-only propagation. Our DoF analysis unifies prior results, and establishes that: (i) multipath captures the best of both LOS-only and NLOS-only propagation, and (ii) under certain geometric configurations of scatterers, multipath can offer significant resolution gains over LOS-only propagation.

Index Terms—Degrees of freedom, multipath, multipath exploitation, resolution analysis, scattering, wireless imaging.

I. INTRODUCTION

TUELED by advances in massive MIMO¹ technology, there has been growing interest lately [3]–[10] in performing *imaging* using traditional communication infrastructure. For the electromagnetic spectrum used in wireless communication, signals suffer from significant multipath due to scattering in the environment. In this context, a natural question arises: how does multipath impact the resolution of wireless imaging systems?

In this paper, we derive fundamental resolution limits for wireless imaging systems in the presence of multipath. We analyze the *passive* system configuration shown in Fig. 1, with an aperture sampling electromagnetic fields backscattered from an imaging scene along both line-of-sight (LOS) and non-LOS (NLOS) paths. The configuration is termed passive because the illumination onto the scene is assumed to be arbitrary, and not under the aperture's control. For the purposes of this work, we assume that the aperture, scene and scatterers remain static for the duration of imaging.

Manuscript received August 25, 2021; revised January 23, 2022 and March 9, 2022. This work was partially supported by the NSF grant CNS-1956297. The material in this paper was presented in part at the IEEE International Symposium on Information Theory (ISIT), Los Angeles, June 2020 [1], and is based on the first author's master's thesis [2].

The authors are with the Department of Electrical and Computer Engineering, Rice University, Houston, TX, 77005, USA. E-mail: {nm30, ashu}@rice.edu.

¹multiple-input multiple-output

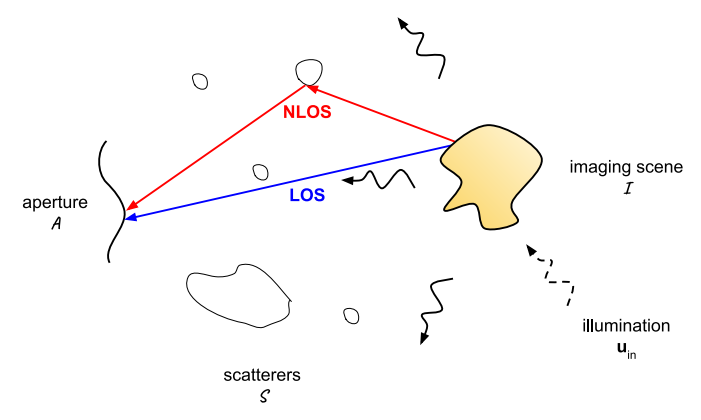


Fig. 1: Analyzed system configuration with an aperture \mathcal{A} sampling fields backscattered from an imaging scene \mathcal{I} in the presence of multipath due to a set of scatterers \mathcal{S} . The dashed arrow represents passive illumination incident onto the scene, and solid arrows represent the resulting backscattered fields.

To characterize the resolution limits in the presence of multipath, we derive the imaging *degrees of freedom* (DoF) corresponding to Fig. 1. The DoF equals the maximum number of points that are *resolvable*, i.e., can be spatially differentiated, in the image reconstruction of the scene [11]–[19]. A higher DoF value implies more resolvable points, and hence smaller (better) resolution. The DoF framework has been used previously to characterize the resolution limits for LOS-only [14], [15], [20]–[23] and NLOS-only [13], [22]–[26] propagation, and more recently in our recent work [18], [19] to quantify resolution-rate trade-offs for dual-function systems performing both imaging and communication with shared resources.

Via the imaging DoF analysis, we make progress towards answering the question: when does multipath offer imaging resolution gains over LOS-only propagation? Prior theoretical [27], [28] and empirical analysis [29]–[36] offer seemingly contradictory answers to this question:

- 1) On the one hand, prior theoretical analysis [27], [28] suggests that given *infinite-sized* apertures, multipath does not improve resolution beyond LOS-only propagation. NLOS propagation simply shapes the singular values of the LOS wireless channel between the aperture and the imaging scene, but does not change the imaging DoF itself. Moreover, in this infinite-sized aperture regime, multipath achieves the Rayleigh resolution limit of $\frac{\lambda}{2}$, for signalling wavelength λ , which is also achievable using LOS-only propagation.
- 2) On the other hand, numerical simulations of multipathexploiting imaging systems [29]–[36] suggest that multipath can significantly improve the resolution compared to LOS-only propagation. Given sufficiently rich scatter-

ing in the environment, it is shown numerically that the Rayleigh resolution limit of $\frac{\lambda}{2}$ is achievable with *finite-sized* apertures. By contrast, achieving the Rayleigh limit is impossible with finite-sized apertures for LOS-only propagation, and requires infinite-sized apertures.

We bridge the gap between these two disparate conclusions by theoretically deriving the imaging DoF in the presence of multipath for *finite-sized* apertures and imaging scenes, and a fixed geometrical configuration of scatterers. Our main result shows that the achievable resolution with multipath, as a fraction of wavelength λ , is inversely proportional to the *total angular interval* subtended by (i) the aperture, and (ii) scatterers, onto the imaging scene. By contrast, the resolution with LOS-only (resp. NLOS-only) propagation depends on the angular interval subtended only by the aperture (resp. scatterers) onto the imaging scene. Thus, multipath is beneficial for imaging when scattering *increases* the angular extent beyond that subtended by the aperture onto the scene.

The two conclusions from prior work [27], [28] and [29]–[36] correspond to two extreme cases of our main result:

- 1) In the infinite-sized aperture regime, the aperture subtends all possible angles onto the imaging scene, e.g., all angles in $[0,\pi]$ for a 1D aperture and scene, which achieves the Rayleigh limit. Note that scattering cannot increase the angular extent beyond LOS-only propagation in this case. Hence, multipath is equivalent to LOS-only propagation, and both multipath and LOS achieve the Rayleigh resolution of $\frac{\lambda}{2}$.
- 2) In the rich scattering regime, the scatterers subtend all possible angles onto the imaging scene, e.g., all angles in $[0,\pi]$ for a 1D aperture and scene, which achieves the Rayleigh limit. Hence, multipath is equivalent to NLOS-only propagation, and achieves the Rayleigh limit with finite-sized apertures. By contrast, LOS-only propagation alone is insufficient to achieve the Rayleigh limit with finite-apertures.

Thus, both sets of conclusions from [27], [28] and [29]–[36] are valid in their respective regimes. Our main result unifies both sets of prior results by showing that the multipath resolution depends on the union of the LOS-only and NLOS-only angular intervals. Thus, multipath effectively captures the best of both LOS-only and NLOS-only propagation.

Taken together, our results highlight the benefits of harnessing multipath in emerging wireless imaging systems. While the benefits of harnessing multipath are well-recognized for communication [37], the same is less true for imaging. Indeed, current state-of-the-art wireless imaging systems [3]–[10] have largely remained limited to LOS-only propagation, and hence have resorted to increasing the aperture size in order to improve the imaging resolution. We hope that the encouraging theoretical results presented in this paper will motivate further research on practical algorithms and system designs that harness the resolution gains provided by multipath.

Finally, we note that a preliminary version of the results in this paper appeared in the conference version of this work [1]. In [1], DoF results were derived assuming single frequency, uni-polarized illumination. Moreover, the results heavily relied

on a functional analytic approximation approach, due to [20], [21], [23], to the DoF computation. In this paper, we significantly expand upon the results of [1] by (i) considering a broadband, arbitrarily polarized system model, and (ii) directly computing the DoF, without resorting to any approximations, by using a combination of well-known electromagnetic theoretic and linear algebraic results. Furthermore, all system-level insights and interpretation of the technical DoF results are new to this paper, and did not appear previously in [1].

The remainder of this paper is organized as follows. In Section II, we present the system model for Fig. 1. We define the imaging DoF and formulate the DoF analysis problem in Section III. We then discuss known results from prior work in Section IV, before presenting our main results in Section V. We conclude the paper in Section VI with discussions and directions for future work. Extensions to cases not covered by our model are briefly discussed in Appendix A.

A. Notation

We use bold uppercase for matrices (e.g., X), bold lowercase for vectors (e.g., x), non-bold lowercase for scalars (e.g., x) and serif uppercase for operators (e.g., X). We denote the column and row spaces of an operator X by col(X) and row (X). Operator composition is denoted by \circ . Sets are represented using calligraphic font (e.g., \mathcal{X}) or capital Greek letters (e.g., Ω). The Lebesgue measure of a set \mathcal{X} is denoted by m(\mathcal{X}). The set union, intersection, and difference operators are \cup , \cap , and \setminus . The $n \times n$ identity matrix is denoted by \mathbf{I}_n . The transpose, conjugate transpose and pseudo-inverse operators are $(\cdot)^{\top}$, $(\cdot)^{\mathsf{H}}$ and $(\cdot)^{\dagger}$ respectively. Vectorization and diagonalization are denoted by vec (\cdot) and diag (\cdot) . The positive part of a scalar x is $[x]^+$. The speed of light is denoted by c.

II. SYSTEM MODEL

Consider the system shown in Fig. 1 with an aperture $\mathcal{A} \subset \mathbb{R}^3$ sampling fields backscattered from an imaging scene $\mathcal{I} \subset \mathbb{R}^3$ in the presence of a collection of scatterers $\mathcal{S} \subset \mathbb{R}^3$. We make the following assumptions on the system operation.

Assumption 1: The aperture A, imaging scene \mathcal{I} and set of scatterers \mathcal{S} remain static for the duration of imaging.

Assumption 2: The imaging scene \mathcal{I} is illuminated by passive fields not under the aperture's control.

In addition to Assumptions 1 and 2, we make the following modeling assumption.

Assumption 3: The aperture A, imaging scene \mathcal{I} and set of scatterers \mathcal{S} all have non-zero Lebesgue measures.

In other words, Assumption 3 implies that we use *continuous*, as opposed to discrete (sampled), models for the aperture, scene and set of scatterers. Moreover, given Assumption 1 holds, our modeling is *deterministic*. This is in contrast to traditional stochastic models for wireless channels, e.g., IID² Rayleigh fading, which are only valid under limiting assumptions on the sampling (e.g., at half-wavelengths) and spatial correlation of measurements (e.g., uncorrelated) at the aperture [16]. Such continuous deterministic models, a.k.a.

²independent and identically distributed

signal space models, have been widely used previously to characterize the resolution limits of imaging [11]–[16] and multiplexing gains of wireless [21]–[23], [38] systems.

To that end, we model the aperture \mathcal{A} as an N-dimensional embedded submanifold of \mathbb{R}^3 , where $N \in \{1,2\}$. Such a representation encompasses most aperture models commonly used in practice, such as linear, planar, cylindrical and spherical apertures. In Fig. 2, we illustrate how different values of N map to different aperture models. We restrict ourselves to $N \in \{1,2\}$ since we are not aware of any practical implementations of volumetric apertures that can be modeled as three-dimensional³ submanifolds of \mathbb{R}^3 .

We are now ready to formalize the system model. Let $\mathbf{r_a} \in \mathbb{R}^3$, $\mathbf{r_i} \in \mathbb{R}^3$ and $\mathbf{r_s} \in \mathbb{R}^3$ respectively denote positions vectors of points on the aperture \mathcal{A} , imaging scene \mathcal{I} and set of scatterers \mathcal{S} . Let $\Omega \subset \mathbb{R}$ denote the bandwidth⁴ of operation. In our system model, we shall represent all electromagnetic fields in \mathbb{C}^3 , i.e., in terms of three orthogonal components. Such a representation is known as the tripole model [16], [22], and allows modeling fields with arbitrary polarization.

For frequencies $\omega \in \Omega$, let $\mathbf{x}(\mathbf{r}_i; \omega) \in \mathbb{C}^3$ denote the current density at position vector \mathbf{r}_i on the scene \mathcal{I} , induced due to incident illumination $\mathbf{u}_{in}(\mathbf{r}_i; \omega) \in \mathbb{C}^3$. The measured field at position vector \mathbf{r}_a on the aperture \mathcal{A} is given by [16], [22]

$$\mathbf{y}\left(\mathbf{r}_{\mathsf{a}};\omega\right) = \int_{\mathcal{I}} \mathbf{H}\left(\mathbf{r}_{\mathsf{a}},\mathbf{r}_{\mathsf{i}};\omega\right) \cdot \mathbf{x}\left(\mathbf{r}_{\mathsf{i}};\omega\right) d\mathbf{r}_{\mathsf{i}} + \mathbf{n}\left(\mathbf{r}_{\mathsf{a}};\omega\right). \quad (1)$$

In (1), $\mathbf{n}(\mathbf{r}_a; \omega) \in \mathbb{C}^3$ denotes the additive noise at the aperture. The current densities $\mathbf{x}(\mathbf{r}_i; \omega)$ may be decomposed in terms of the incident illumination $\mathbf{u}_{in}(\mathbf{r}_i; \omega)$ as [16], [22]

$$\mathbf{x}(\mathbf{r}_{i};\omega) = \operatorname{diag}(\mathbf{u}_{in}(\mathbf{r}_{i};\omega)) \cdot \mathbf{f}(\mathbf{r}_{i};\omega),$$
 (2)

corresponding to the element-wise product between the incident illumination $\mathbf{u}_{in}\left(\mathbf{r}_{i};\omega\right)$ and the scene *reflectivities* $\mathbf{f}\left(\mathbf{r}_{i};\omega\right)$. As the name suggests, the reflectivities model the reflective response of points in the scene to incident fields. As we shall formalize shortly in Section III, the goal of imaging is to recover the reflectivities $\mathbf{f}\left(\mathbf{r}_{i};\omega\right)$ from the aperture measurements $\mathbf{y}\left(\mathbf{r}_{a};\omega\right)$.

The term $\mathbf{H}(\mathbf{r_a},\mathbf{r_i};\omega)\in\mathbb{C}^{3\times3}$ in (1) denotes the frequency-domain channel response, a.k.a. *Green's function*, between points on the aperture and imaging scene. In free space with LOS-only propagation, the Green's function takes the form [16], [22]

$$\mathbf{H}_{LOS}(\mathbf{r}_{\mathsf{a}}, \mathbf{r}_{\mathsf{i}}; \omega) = \left(j \frac{\omega}{c} \eta\right) \cdot \frac{e^{-j \frac{\omega}{c} \|\mathbf{r}_{\mathsf{a}\mathsf{i}}\|_{2}}}{4\pi \|\mathbf{r}_{\mathsf{a}\mathsf{i}}\|_{2}} \left(\mathbf{I}_{3} - \hat{\mathbf{r}}_{\mathsf{a}\mathsf{i}} \cdot \hat{\mathbf{r}}_{\mathsf{a}\mathsf{i}}^{\mathsf{H}}\right), \quad (3)$$

$$\mathbf{r}_{\mathsf{a}\mathsf{i}} = \mathbf{r}_{\mathsf{a}} - \mathbf{r}_{\mathsf{i}}, \quad \hat{\mathbf{r}}_{\mathsf{a}\mathsf{i}} = \frac{\mathbf{r}_{\mathsf{a}\mathsf{i}}}{\|\mathbf{r}_{\mathsf{a}\mathsf{i}}\|_{2}}. \quad (4)$$

In (3), c denotes the speed of light, η denotes the intrinsic impedance of free space, \mathbf{I}_n denotes the $n \times n$ identity matrix and $(\cdot)^{\mathsf{H}}$ denotes the complex conjugate.

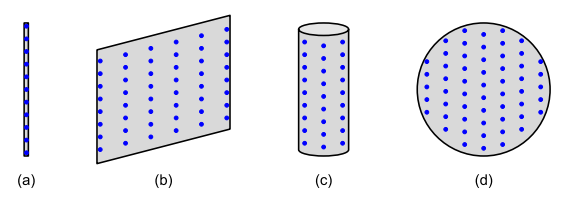


Fig. 2: Illustration of different apertures \mathcal{A} modeled as N-dimensional embedded submanifolds of \mathbb{R}^3 . (a) Linear aperture (N=1). (b) Planar aperture (N=2). (c) Cylindrical aperture (N=2). (d) Spherical aperture (N=2). The blue dots represent example locations of antennas on the apertures.

Since our goal in this paper is to analyze the case shown in Fig. 1 with both LOS and NLOS propagation, we consider the following Green's function in our analysis,

$$\mathbf{H}\left(\mathbf{r}_{\mathsf{a}}, \mathbf{r}_{\mathsf{i}}; \omega\right) = \mathbf{H}_{\mathsf{LOS}}\left(\mathbf{r}_{\mathsf{a}}, \mathbf{r}_{\mathsf{i}}; \omega\right) + \mathbf{H}_{\mathsf{NLOS}}\left(\mathbf{r}_{\mathsf{a}}, \mathbf{r}_{\mathsf{i}}; \omega\right), \quad (5)$$

with the NLOS Green's function $\mathbf{H}_{NLOS}(\mathbf{r}_a, \mathbf{r}_i; \omega)$ given by

$$\mathbf{H}_{\mathsf{NLOS}}(\mathbf{r}_{\mathsf{a}}, \mathbf{r}_{\mathsf{i}}; \omega) = \int_{\mathcal{S}} \mathbf{H}_{\mathsf{LOS}}(\mathbf{r}_{\mathsf{a}}, \mathbf{r}_{\mathsf{s}}; \omega) \cdot \mathsf{diag}(\mathbf{h}(\mathbf{r}_{\mathsf{s}}; \omega)) \cdot \mathbf{H}_{\mathsf{LOS}}(\mathbf{r}_{\mathsf{s}}, \mathbf{r}_{\mathsf{i}}; \omega) \, \mathsf{d}\mathbf{r}_{\mathsf{s}}. \quad (6)$$

The three terms inside the integral in (6) correspond to (i) radiation from the imaging scene to the set of scatterers \mathcal{S} , modeled via $\mathbf{H}_{LOS}(\mathbf{r}_s, \mathbf{r}_i; \omega)$, (ii) interaction with the scatterers, modeled in terms of the scatterer reflectivities $\mathbf{h}(\mathbf{r}_s; \omega) \in \mathbb{C}^3$, and (iii) reception at the aperture from the scatterers, modeled via $\mathbf{H}_{LOS}(\mathbf{r}_a, \mathbf{r}_s; \omega)$.

By definition, $\mathbf{H}_{\text{NLOS}}(\mathbf{r}_{\mathsf{a}},\mathbf{r}_{\mathsf{i}};\omega)$ in (6) models single-bounce isotropic scattering. Extensions to multiple bounces (all the way up to infinite bounces) are quite straightforward, and are derived in Appendix A. We also show in Appendix A that the extension of (6) to multiple bounces does not change our main results. Moreover, as per the main results of [24], the DoF results remain unchanged even for specular scattering. Hence, for the bulk of this paper, we shall restrict ourselves to the single-bounce NLOS Green's function in (6).

In the next section, we formulate the problem of imaging in the context of (1) and define the degrees of freedom metric we use to analyze the resolution limits for our system model.

III. PROBLEM FORMULATION

Our main goal in this paper is to characterize the resolution limits for imaging in the presence of multipath. Specifically, we answer the following question:

Given a *constraint* on the spatial sizes of the aperture \mathcal{A} and scene \mathcal{I} , and a *fixed* geometrical configuration of scatterers in \mathcal{S} , what is the achievable imaging resolution for the case with *both* LOS and NLOS propagation in (1)?

As outlined in (Q), we will derive the resolution limits for our model assuming *bounded* Lebesgue measures of the aperture \mathcal{A} , imaging scene \mathcal{I} and operating bandwidth Ω . We will use the imaging degrees of freedom (DoF), defined shortly below, as the metric of choice in our analysis.

To that end, we first define some notation below that will help us in formalizing the notion of imaging.

³labeling cylindrical or spherical apertures as 3D is a misnomer since they are both 2D submanifolds embedded in 3D Euclidean space (\mathbb{R}^3)

⁴for notational ease, we shall only consider angular frequency and bandwidth, i.e., frequency $\equiv \omega = 2\pi f$ and bandwidth $\equiv \Omega = 2\pi W$

Notation: Let \mathcal{X} denote the space of all current densities $\mathbf{x}(\mathbf{r}_i;\omega)$ from (2) supported over the imaging scene (in space) and bandwidth (in frequency),

$$\mathcal{X} = \{ \mathbf{x} (\mathbf{r}_i; \omega) : \mathbf{r}_i \in \mathcal{I}, \ \omega \in \Omega \}. \tag{7}$$

Analogously, let \mathcal{F} denote the space of all scene reflectivities $\mathbf{f}(\mathbf{r}_i; \omega)$ from (2),

$$\mathcal{F} = \{ \mathbf{f} (\mathbf{r}_i; \omega) : \mathbf{r}_i \in \mathcal{I}, \ \omega \in \Omega \}.$$
 (8)

Similarly, let \mathcal{Y} denote the space of aperture measurements,

$$\mathcal{Y} = \{ \mathbf{y} (\mathbf{r}_{\mathsf{a}}; \omega) : \mathbf{r}_{\mathsf{a}} \in \mathcal{A}, \ \omega \in \Omega \}. \tag{9}$$

Finally, for any operator $T: \mathcal{V} \to \mathcal{W}$, we use col(T) and row(T) to denote its column and row spaces,

$$\begin{aligned} \text{col}\left(T\right) &= T\left(\mathcal{V}\right) \subseteq \mathcal{W},\\ \text{row}\left(T\right) &= \left\{\mathbf{v} \in \mathcal{V} : T\left(\mathbf{v}\right) \neq \mathbf{0}\right\} \subseteq \mathcal{V}. \end{aligned}$$

We now define imaging as the operation of estimating the reflective response of points in the imaging scene \mathcal{I} , i.e., recovering the reflectivities $\mathbf{f}(\mathbf{r}_i;\omega)$, from the aperture measurements $\mathbf{y}(\mathbf{r}_a;\omega)$.

Definition 1 (Imaging): Let $H : \mathcal{X} \to \mathcal{Y}$ denote the operator corresponding to the integral mapping in (1), such that

$$\mathbf{y}\left(\mathbf{r}_{\mathsf{a}};\omega\right)=\mathsf{H}\left(\mathbf{x}\left(\mathbf{r}_{\mathsf{i}};\omega\right)\right)=\int_{\mathcal{I}}\mathbf{H}\left(\mathbf{r}_{\mathsf{a}},\mathbf{r}_{\mathsf{i}};\omega\right)\cdot\mathbf{x}\left(\mathbf{r}_{\mathsf{i}};\omega\right)\mathsf{d}\mathbf{r}_{\mathsf{i}}.$$

Then, imaging corresponds to a compact⁵ operator $A: \mathcal{Y} \to \mathcal{F}$ that maps aperture measurements to reflectivity estimates. We can now define the space of reconstructions $\hat{\mathcal{F}}$ produced by A, with outputs of operator H as its inputs,

$$\hat{\mathcal{F}} = A(H(\mathcal{X})) = col(A \circ H) \subset \mathcal{F},$$

where o denotes operator composition.

To define imaging resolution and DoF, we shall characterize the *dimensionality* of the space $\hat{\mathcal{F}}$. Before presenting formal definitions, we illustrate the high-level connections between dimensionality and resolution via the following example.

Example 1: Consider a 1D setting with the interval [0,1] representing the support $\mathcal{I} \times \Omega$. In this setting, reflectivities $\mathbf{f}(\mathbf{r}_i;\omega)$ are represented by 1D functions, $f(x): x \in [0,1]$.

The connection between the resolution and dimensionality is via Shannon's sampling theorem. To illustrate, consider the space \mathcal{F} of all reflectivities supported over [0,1]. Without any additional constraints, the space \mathcal{F} is infinite-dimensional since any arbitrary reflectivity f(x) can be decomposed into an infinite number of weighted delta functions. In the context of imaging, the resolution is zero since any two point sources separated by $\ell \in (0,1]$ are distinguishable.

On the other hand, consider the space $\hat{\mathcal{F}}$ of reconstructions $\hat{f}(x)$ that can be expressed as a convolution of reflectivities f(x) with a sinc bandlimited to $[-\Delta, +\Delta]$,

$$\hat{f}(x) = f(x) * \frac{\Delta}{\pi} \operatorname{sinc}(\Delta \cdot x).$$

 $^5{\rm an}$ operator T is compact if for any bounded sequence of inputs $\{f_n\},$ $\{\mathsf{T}f_n\}$ contains a convergent bounded sequence

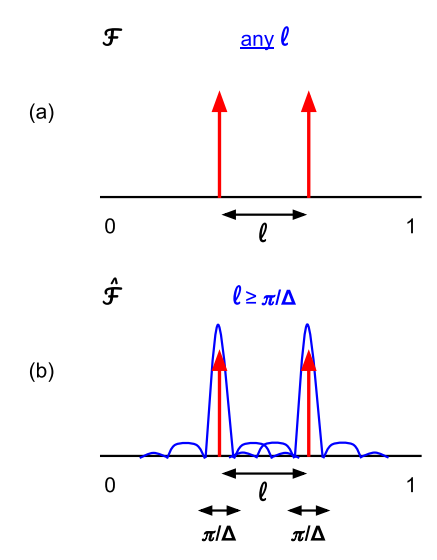


Fig. 3: Illustration of Example 1 to describe high-level connections between dimensionality and imaging resolution. (a) Consider infinite-dimensional space $\mathcal F$ of 1D functions supported over [0,1]. Two point sources separated by $\ell\in(0,1]$ are resolvable from their sum for $all\ \ell\in(0,1]$, i.e., the resolution is zero. (b) Consider $\frac{\Delta}{\pi}$ -dimensional space $\hat{\mathcal F}$ of convolutions of 1D functions with a sinc bandlimited to $[-\Delta,+\Delta]$. Two point sources separated by $\ell\in(0,1]$ are resolvable from their sum only when $\ell\geq\frac{\pi}{\Delta}$, i.e., the resolution is $\frac{\pi}{\Delta}$.

The space $\hat{\mathcal{F}}$ is $\frac{\Delta}{\pi}$ -dimensional as per Shannon's well-known 2WT formula. Moreover, two point sources must separated by at least $\ell \geq \frac{\pi}{\Delta}$ to be distinguishable, i.e., the imaging resolution is $\frac{\pi}{\Delta}$. In other words, the finite-dimensionality of $\hat{\mathcal{F}}$ implies non-zero resolution. We illustrate both cases described above in Fig. 3.

We now formally define dimensionality, DoF and resolution. Definition 2 (Set Dimensionality [16], [39]): Consider a subset \mathcal{A} of a normed linear space \mathcal{X} with unit norm signals. The dimensionality of \mathcal{A} equals the smallest value of n such that \mathcal{A} can be approximated arbitrarily well by any n-dimensional subspace \mathcal{X}_n of \mathcal{X} ,

$$\dim (\mathcal{A}) = \min \left\{ n : \rho_n \left(\mathcal{A} \right) = 0 \right\},\,$$

where $\rho_n(A)$ is called the *Kolmogorov n-width*,

$$\rho_{n}\left(\mathcal{A}\right) = \inf_{\mathcal{X}_{n} \subseteq \mathcal{X}} \sup_{f \in \mathcal{A}} \inf_{g \in \mathcal{X}_{n}} \left\| f - g \right\|.$$

In other words, the dimensionality of a set equals the minimum number of independent basis elements required to approximate it up to arbitrarily small accuracy.

Definition 3 (Imaging DoF [18], [19]): The imaging DoF, d_{img} , corresponds to the dimensionality of $\hat{\mathcal{F}}$, normalized to unit norm for consistency with Definition 2,

$$\mathsf{d}_{\mathsf{img}} = \mathsf{dim}\left(\hat{\mathcal{F}}\right) = \min\left\{n : \rho_n\left(\hat{\mathcal{F}}\right) = 0\right\}.$$

We note that Definition 3 associates a DoF value to the image $\hat{\mathcal{F}}$ of a given imaging operator A, and hence is analogous to specifying the rate of a particular coding scheme. Similar to the notion of achievability in information theory, we define the notion of an *achievable* imaging DoF below.

Definition 4 (Achievable DoF [18], [19]): An imaging DoF of d_{img} is achievable if there exists an imaging operator A s.t.

$$\mathsf{d}_{\mathsf{img}} = \mathsf{dim}\left(\mathsf{A}\left(\mathsf{H}\left(\mathcal{X}\right)\right)\right) = \mathsf{dim}\left(\hat{\mathcal{F}}\right),$$

where H is the operator corresponding to (1) from Definition 1. We now define the notion of imaging resolution.

Definition 5 (Imaging Resolution): Given an imaging DoF of dimg is achievable for a scene and operating bandwidth with bounded Lebesgue measures, $m(\mathcal{I}) < \infty$, $m(\Omega) < \infty$, all 4D tuples $(\delta_x, \delta_y, \delta_z, \delta_\omega)$ that satisfy

$$\beta_d \cdot \left(\frac{\delta_x}{2}\right) \cdot \left(\frac{\delta_y}{2}\right) \cdot \left(\frac{\delta_z}{2}\right) \cdot \left(\frac{\delta_\omega}{2}\right) = \frac{\mathsf{m}\left(\mathcal{I} \times \Omega\right)}{\mathsf{d}_{\mathsf{img}}},$$

constitute a set of feasible imaging resolution values in space (along the x-, y- and z-axes) and frequency. In the equation above, $d \in \{1, 2, 3\}$ denotes the dimensionality of \mathcal{I} , and β_d denotes the volume of the d-dimensional unit ball,

$$\beta_d = \frac{\pi^{\frac{d}{2}}}{\Gamma\left(\frac{d}{2} + 1\right)},$$

where $\Gamma(\cdot)$ is the gamma function.

In other words, the imaging DoF d_{img} equals the number of resolution-limited ellipsoids that can be packed in spacefrequency into the support $\mathcal{I} \times \Omega$. The principal diameters of the ellipsoid correspond to the spatial and spectral resolution. For instance, consider Example 1, where d = 1 and single frequency illumination such that $\mathcal{I} \times \Omega = \mathcal{I} = [0, 1]$. Thus, $\beta_d=2$ and $\delta=\frac{1}{d_{img}}=\frac{\pi}{\Delta}.$ On the other hand, consider imaging a 3D scene with single frequency illumination, d=3and $\mathcal{I} \times \Omega = \mathcal{I}$. In this case, the spatial resolution satisfy

$$\frac{4\pi}{3} \cdot \left(\frac{\delta_x}{2}\right) \cdot \left(\frac{\delta_y}{2}\right) \cdot \left(\frac{\delta_z}{2}\right) = \frac{\mathsf{m}\left(\mathcal{I}\right)}{\mathsf{d}_{\mathsf{img}}},$$

which corresponds to packing the 3D imaging scene \mathcal{I} with $\mathsf{d}_{\mathsf{img}}$ number of 3D ellipsoids of radii $\frac{\delta_x}{2}$, $\frac{\delta_y}{2}$ and $\frac{\delta_z}{2}$.

In the next section, we discuss known results from prior work on the DoF with LOS-only, NLOS-only and multipath propagation. We present our main results for the system model in (1) later in Section V.

IV. KNOWN RESULTS

We first discuss known results on the LOS-only and NLOSonly DoF in Theorem 1, and illustrate them for a simple linear aperture and imaging scene model that brings forth key system-level insights while remaining analytically tractable. We then present prior results on multipath in Theorem 2, which have led to two seemingly contradictory conclusions in the literature. We resolve the contradiction between the two results of Theorem 2 via our main results in Section V.

All results in this section and the next are presented in terms of the angular domain notation from [22], [24], which associates angular intervals with every point on the aperture, scatterers and imaging scene. To that end, let Ψ_{ia} (resp. Ψ_{sa}) denote the angular interval subtended by the imaging scene \mathcal{I} (resp. scatterers S) onto the aperture A. The angular intervals subtended onto the scene \mathcal{I} are defined analogously as Ψ_{ai} and Ψ_{si} . The notation is illustrated in Fig. 4. The Lebesgue

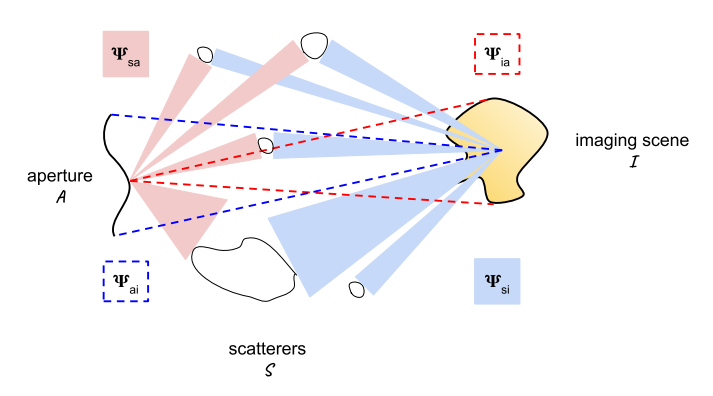


Fig. 4: Illustration of angular domain notation for same system configuration as in Fig. 1. The variables Ψ_{ia} , Ψ_{ai} , Ψ_{sa} and Ψ_{si} respectively denote the angular intervals subtended by imaging scene onto aperture, aperture onto imaging scene, scatterers onto aperture and scatterers onto imaging scene.

measures of Ψ_{ia} , Ψ_{ai} , Ψ_{sa} and Ψ_{si} are given by their solid angles [22],

$$\mathbf{m}\left(\Psi\right) = \int_{\Psi} \sin\theta \mathrm{d}\theta \mathrm{d}\phi, \ \forall \Psi \in \left\{\Psi_{\mathsf{ia}}, \Psi_{\mathsf{ai}}, \Psi_{\mathsf{sa}}, \Psi_{\mathsf{si}}\right\}. \tag{10}$$

Similarly, we shall use the notion of the *effective* Lebesgue measures [22] of the aperture and scene, $m_{eff}(\cdot)$, in all results. The effective Lebesgue measure of the aperture (resp. scene) is defined as the area of its projection onto a 2D plane parallel to the scene (resp. aperture). For instance, $m_{eff}(A) = L$ for a linear aperture of length L, $m_{eff}(A) = L_1L_2$ for a $L_1 \times L_2$ sized planar aperture, $m_{eff}(A) = 2rh$ for a cylindrical aperture of radius r, height h, and $m_{eff}(A) = \pi r^2$ for a spherical aperture of radius r.

A. Prior Results on LOS-only & NLOS-only DoF

The following theorem reviews known results on the LOSonly and NLOS-only DoF.

Theorem 1 (LOS-only & NLOS-only DoF [13]-[15], [20]-[26]): Let H_{LOS} and H_{NLOS} denote the operators as per Definition 1 for the LOS Green's function from (3) and NLOS Green's function from (6) respectively. Define transmit and receive spaces \mathcal{X} and \mathcal{Y} as in (7) and (9).

- 1) The operators $\mathsf{H}_{\mathsf{LOS}}$ and $\mathsf{H}_{\mathsf{NLOS}}$ are compact. 2) Define the set $\Omega^{(k)} = \left\{ \omega^k : \omega \in \Omega \right\}$, and let $\mathcal{T} \subset \mathbb{R}$ denote the time interval over which the aperture measurements are acquired. Then, the LOS and NLOS transmit and receive spaces, \mathcal{X}_i and \mathcal{Y}_i , $j \in \{LOS, NLOS\}$, have dimensionalities

$$\begin{split} & \dim \left(\mathcal{X}_{j}\right) = \left(\frac{\mathsf{m}\left(\mathcal{T}\right)\mathsf{m}\left(\Omega^{(N+1)}\right)}{\pi}\right) \left(\frac{B_{j}}{\left(2\pi c\right)^{N}\left(N+1\right)}\right), \\ & \dim \left(\mathcal{Y}_{j}\right) = \left(\frac{\mathsf{m}\left(\mathcal{T}\right)\mathsf{m}\left(\Omega^{(N+1)}\right)}{\pi}\right) \left(\frac{A_{j}}{\left(2\pi c\right)^{N}\left(N+1\right)}\right), \\ & A_{\mathsf{LOS}} = \mathsf{m}_{\mathsf{eff}}\left(\mathcal{A}\right)\mathsf{m}\left(\Psi_{\mathsf{ia}}\right), \ A_{\mathsf{NLOS}} = \mathsf{m}_{\mathsf{eff}}\left(\mathcal{A}\right)\mathsf{m}\left(\Psi_{\mathsf{sa}}\right), \\ & B_{\mathsf{LOS}} = \mathsf{m}_{\mathsf{eff}}\left(\mathcal{I}\right)\mathsf{m}\left(\Psi_{\mathsf{ai}}\right), \ B_{\mathsf{NLOS}} = \mathsf{m}_{\mathsf{eff}}\left(\mathcal{I}\right)\mathsf{m}\left(\Psi_{\mathsf{si}}\right), \end{split}$$

assuming the bandwidth Ω has non-zero measure, $m(\Omega) > 0$.

In other words, the transmit and receive space dimensionalities correspond to the product of the effective aperture or imaging scene size and the angular interval subtended by the LOS or NLOS environment. In the special case of single frequency illumination, $\Omega = \{\omega_0\}$,

$$\begin{split} \dim\left(\mathcal{X}_{\mathbf{j}}\right) &= \left(\frac{2B_{\mathbf{j}}\omega_{0}^{N}}{\left(2\pi c\right)^{N}}\right), \; \mathbf{j} \in \left\{\mathsf{LOS}, \mathsf{NLOS}\right\}, \\ \dim\left(\mathcal{Y}_{\mathbf{j}}\right) &= \left(\frac{2A_{\mathbf{j}}\omega_{0}^{N}}{\left(2\pi c\right)^{N}}\right), \; \mathbf{j} \in \left\{\mathsf{LOS}, \mathsf{NLOS}\right\}, \end{split}$$

where the multiplicative factor 2 is the gain from polarization [22], and equals the rank of the $\left(\mathbf{I}_{3}-\hat{\mathbf{r}}_{ai}\cdot\hat{\mathbf{r}}_{ai}^{H}\right)$ term in (3).

 The achievable DoF is d_{img} = dim (col (H_j)), which equals the minimum of the transmit and receive space dimensionalities,

$$\begin{split} \mathsf{d}_{\mathsf{img}} &= \mathsf{dim}\left(\mathsf{col}\left(\mathsf{H}_{\mathsf{j}}\right)\right) = N_{\mathsf{j}} + o\left(N_{\mathsf{j}}\right), \ \mathsf{j} \in \left\{\mathsf{LOS}, \mathsf{NLOS}\right\}, \\ N_{\mathsf{j}} &= \min\left\{\mathsf{dim}\left(\mathcal{X}_{\mathsf{j}}\right), \mathsf{dim}\left(\mathcal{Y}_{\mathsf{j}}\right)\right\}. \end{split}$$

The achievability of $d_{img} = dim \left(col \left(H_j \right) \right)$ follows from the compactness of imaging operator A,

$$d_{img} = \dim (col (A \circ H_i)) \le \dim (col (H_i)), \qquad (11)$$

and the bound is achieved using the pseudo-inverse, $A = H_i^{\dagger}$.

4) NLOS DoF is unchanged with multi-bounce scattering.

B. Illustration of Theorem 1

Before proceeding, we illustrate Theorem 1 for a linear aperture and scene, which will also be used to illustrate other upcoming results. The analyzed example captures the key system-level insights of our analysis while remaining analytically tractable. Extensions of our analysis to more complicated aperture models from Fig. 2 are straightforward, but cumbersome, and are thus not presented for the sake of clarity.

Example 2: Consider a linear aperture of length $L_{\rm a}$ imaging a linear scene of length $L_{\rm i}$ at a distance D. The mismatch in orientation between the aperture and scene is modeled by the angle $\theta_{\rm o} \in [-\frac{\pi}{2}, +\frac{\pi}{2}]$. The example is illustrated in Figures 5 and 6 for LOS-only and NLOS-only propagation.

For this example, we have N=1 and

$$\mathsf{m}_{\mathsf{eff}}\left(\mathcal{A}\right) = L_{\mathsf{a}}\cos\theta_{\mathsf{o}},\tag{12}$$

$$\mathsf{m}_{\mathsf{eff}}\left(\mathcal{I}\right) = L_{\mathsf{i}}\cos\theta_{\mathsf{o}},\tag{13}$$

$$\mathsf{m}\left(\Psi_{\mathsf{ia}}\right) = 2\sin\left(\tan^{-1}\left(\frac{L_{\mathsf{i}}}{2D}\right)\right) \approx \frac{L_{\mathsf{i}}}{D},$$
 (14)

$$\label{eq:psi} \mathsf{m}\left(\Psi_{\mathsf{a}\mathsf{i}}\right) = 2\sin\left(\tan^{-1}\left(\frac{L_{\mathsf{a}}}{2D}\right)\right) \approx \frac{L_{\mathsf{a}}}{D}, \tag{15}$$

where the small-angle approximation holds for L_i , $L_a \leq \frac{D}{2}$. Let $\Omega = [-\omega_0 - \pi W, -\omega_0 + \pi W] \cup [\omega_0 - \pi W, \omega_0 + \pi W]$ and $\mathcal{T} = [0, T]$. Thus, as per Theorem 1, for all W > 0,

$$N_{\text{LOS}} \approx 2WT \cdot \left(\frac{2L_{\text{a}}L_{\text{i}}\cos\theta_{\text{o}}}{\lambda_0 D}\right),$$
 (16)

$$N_{\mathsf{NLOS}} = 2WT \cdot \left(\frac{2\cos\theta_{\mathsf{o}}}{\lambda_{\mathsf{0}}} \min\left\{L_{\mathsf{a}}\mathsf{m}\left(\Psi_{\mathsf{sa}}\right), L_{\mathsf{i}}\mathsf{m}\left(\Psi_{\mathsf{si}}\right)\right\}\right), \quad (17)$$

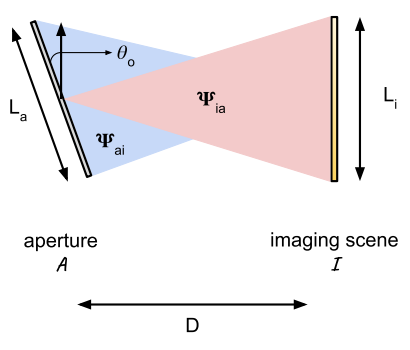


Fig. 5: Illustration of Example 2, which will be used throughout to illustrate main results. System configuration consists of a linear aperture of length $L_{\rm a}$ imaging a linear scene of length $L_{\rm i}$ at a distance D. The mismatch in orientation between the aperture and scene is modeled by the angle $\theta_{\rm o} \in [-\frac{\pi}{2}, +\frac{\pi}{2}]$. Depicted configuration is LOS-only with angular intervals $\Psi_{\rm ia}$, $\Psi_{\rm ai}$ subtended by imaging scene onto aperture and vice versa.

where $\lambda_0 = \frac{2\pi c}{\omega_0}$ is the wavelength corresponding to ω_0 . Moreover, DoFs are given by the terms in parenthesis above in the special case of W=0, i.e., single frequency illumination.

To gain some intuition for (16) and (17), let us consider the LOS and NLOS DoFs separately.

- 1) LOS DoF: We shall analyze the effects of: (i) bandwidth W, (ii) polarization, (iii) misorientation angle θ_o , (iv) sampling at the aperture and its size L_a , on the LOS DoF.
- (i) Ignoring the $o(\cdot)$ term⁶, the DoF equals the product of the temporal DoF, given by Shannon's well-known 2WT formula, and the spatial DoF, given by the term in parenthesis in (16). Thus, the spatial resolution is *independent* of the bandwidth W, and only depends on the center frequency ω_0 . Similarly, the spectral resolution depends only on T. This can be shown via Definition 5,

$$\beta_d \cdot \left(\frac{\delta}{2}\right) \cdot \left(\frac{\delta_\omega}{2}\right) = \frac{\delta \cdot \delta_\omega}{2} \approx \frac{\mathsf{m}\left(\mathcal{I} \times \Omega\right)}{N_{\mathsf{LOS}}},$$
 (18)

$$\delta \approx \frac{\mathsf{m}\left(\mathcal{I}\right)}{\left(\frac{L_{\mathsf{a}}L_{\mathsf{i}}\cos\theta_{\mathsf{o}}}{\lambda_{0}D}\right)} = \frac{\lambda_{0}D}{L_{\mathsf{a}}\cos\theta_{\mathsf{o}}},\tag{19}$$

$$\delta_{\omega} = \frac{\mathsf{m}\left(\Omega\right)}{2WT} = \frac{2\pi}{T},\tag{20}$$

where d=1 and $\beta_d=2$ since the imaging scene \mathcal{I} is 1D.

- (ii) The DoF gain due to polarization is the factor 2 in the parenthesis in (16) [22], [40]. However, this gain does *not* affect the spatio-spectral resolution in (19) and (20) since it gets effectively canceled out by the factor 2 in the denominator of the left hand side in (18). This is so since the resolution in Definition 5 is only defined in space-frequency. Polarization, being an orthogonal resource in addition to space-frequency, has no effect on the spatio-spectral resolution.
- (iii) The $\frac{1}{\cos\theta_o}$ factor in (19) captures the effect of misorientation. Specifically, the best-case corresponds to $\theta_o = 0$, with $\delta = \frac{\lambda_0 D}{L_a}$, whereas $\theta_o = \pm \frac{\pi}{2}$ is the worst-case, with $\delta = \infty$.
- (iv) Via (19), larger aperture sizes L_a lead to smaller resolution δ . Thus, δ is lower bounded by the resolution correspond-

⁶the term can be safely ignored in the limit of large SNR and large aperture and imaging scene sizes [16], [22], [24]

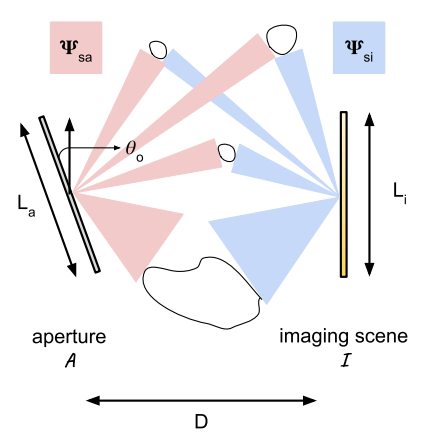


Fig. 6: Illustration of Example 2 with NLOS-only propagation and scattering angular intervals Ψ_{sa} and Ψ_{si} subtended onto aperture and imaging scene respectively.

ing to infinite aperture size, $L_{\rm a} \to \infty$. In the limit $L_{\rm a} \to \infty$, the term $\frac{L_{\rm a}}{D}$ is replaced by $\lim_{L_{\rm a} \to \infty} 2 \sin \left(\tan^{-1} \left(\frac{L_{\rm a}}{2D} \right) \right) = 2$. The lower bound on δ is thus

$$\delta \ge \frac{\lambda_0}{2\cos\theta_0} \ge \frac{\lambda_0}{2},\tag{21}$$

where the Rayleigh resolution, $\frac{\lambda_0}{2}$, corresponds to $\theta_0 = 0$. Analogously, the optimal aperture sampling, defined as

$$\delta_{\mathsf{a}} = \frac{\mathsf{m}\left(\mathcal{A}\right)}{\left(\frac{L_{\mathsf{a}}L_{\mathsf{i}}\cos\theta_{\mathsf{o}}}{\lambda_{0}D}\right)},\tag{22}$$

can be lower bounded by the infinite scene size case, $L_i \to \infty$,

$$\delta_{\mathsf{a}} pprox rac{\lambda_0 D}{L_{\mathsf{i}} \cos \theta_{\mathsf{o}}} \ge rac{\lambda_0}{2 \cos \theta_{\mathsf{o}}} \ge rac{\lambda_0}{2}.$$
 (23)

For finite scene sizes and non-zero misorientation angle θ_o , we see that the optimal aperture sampling is *larger* than the oft-used half-wavelength aperture spacing of $\frac{\lambda_0}{2}$. Thus, while half-wavelength spacing is sufficient to capture all the DoF in the system, it is redundant in most practical use-cases. Similar results hold even with multipath, as we shall see shortly.

- 2) NLOS DoF: The effects of bandwidth W, polarization and misorientation angle $\theta_{\rm o}$ on the DoF in (17) remain unchanged compared to the LOS-only case in (16). Thus, the interesting effects to analyze here are: (i) scattering angular intervals $\Psi_{\rm sa}$ and $\Psi_{\rm si}$, and (ii) aperture and imaging scene sizes, $L_{\rm a}$ and $L_{\rm i}$.
- (i) Consider the special case of *rich scattering* with $\Psi_{sa} = \Psi_{si} = [0, \pi]$, i.e., $m(\Psi_{sa}) = m(\Psi_{si}) = 2$. In this case, the spatial resolution, δ , and optimal aperture sampling, δ_a , defined similar to (19) and (22), equal

$$\delta = \frac{\lambda_0}{2\cos\theta_{\rm o}} \cdot \frac{L_{\rm i}}{\min\left\{L_{\rm a}, L_{\rm i}\right\}} \ge \frac{\lambda_0}{2\cos\theta_{\rm o}}, \tag{24}$$

$$\delta_{\mathsf{a}} = \frac{\lambda_0}{2\cos\theta_{\mathsf{o}}} \cdot \frac{L_{\mathsf{a}}}{\min\{L_{\mathsf{a}}, L_{\mathsf{i}}\}} \ge \frac{\lambda_0}{2\cos\theta_{\mathsf{o}}}.\tag{25}$$

In contrast to the LOS-only case, the lower bounds in (24) and (25) are achieved with *finite* aperture and scene sizes, when the aperture and imaging scene sizes are equal, $L_{\rm a}=L_{\rm i}$. The difference between the aperture size $L_{\rm a}$ required to

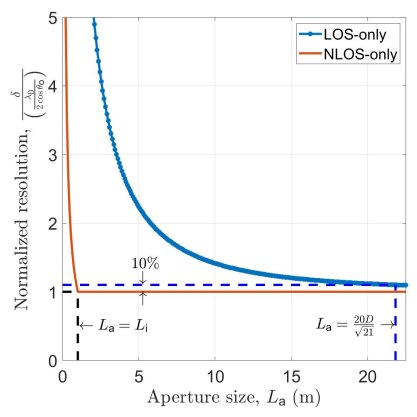


Fig. 7: Normalized resolution $\frac{\delta}{\left(\frac{\lambda_0}{2\cos\theta_0}\right)}$ vs aperture size $L_{\rm a}$ for LOS-only and NLOS-only propagation in a rich scattering indoor environment. System corresponds to Fig. 6 with parameters: imaging scene size $L_{\rm i}=1$ m, distance D=5 m, and scattering angular interval measures, m $(\Psi_{\rm sa})={\rm m}\,(\Psi_{\rm si})=2$. Required aperture size $L_{\rm a}$ for achieving Rayleigh limit up to 10% error with LOS-only propagation is $L_{\rm a}=\frac{20D}{\sqrt{21}}=21.8218$ m, which is $>20\times$ larger compared to $L_{\rm a}=L_{\rm i}=1$ m required with NLOS-only propagation. Therefore, NLOS-only \gg LOS-only propagation in this regime.

achieve the Rayleigh limit with LOS-only and NLOS-only propagation is thus huge. For instance, consider imaging a $L_{\rm i}=1$ m wide imaging scene at a distance of D=5 m, which are typical parameters for an indoor environment, e.g., a conference room. In Fig. 7, we plot the normalized resolution $\frac{\delta}{\left(\frac{\lambda_0}{2\cos\theta_0}\right)}$ vs aperture size $L_{\rm a}$, for LOS-only and NLOS-only propagation in this case. As the plot illustrates, the required aperture size for achieving the Rayleigh limit up to 10% error with LOS-only propagation is $>20\times$ larger compared to that for NLOS-only propagation. Thus, sufficiently rich scattering can drastically improve the resolution with practical finite-sized apertures compared to LOS-only propagation.

(ii) Consider the infinite-sized aperture case, $L_{\rm a} \to \infty$, with limited scattering in the environment, ${\rm m}\left(\Psi_{\rm sa}\right) < 2, \ {\rm m}\left(\Psi_{\rm si}\right) < 2$. In this case, the spatial resolution δ satisfies,

$$\delta = \frac{\lambda_0}{\mathsf{m}(\Psi_{\mathsf{si}})\cos\theta_{\mathsf{o}}} \ge \frac{\lambda_0}{2\cos\theta_{\mathsf{o}}}.\tag{26}$$

Compare (26) to (21) for LOS-only propagation. With NLOS-only propagation, infinite aperture size is *insufficient* to achieve the lower bound of $\frac{\lambda_0}{2\cos\theta_0}$. By contrast, infinite aperture size achieves $\frac{\lambda_0}{2\cos\theta_0}$ resolution in the LOS-only case.

The two cases (i) and (ii) above illustrate the two key regimes in which NLOS-only and LOS-only propagation are respectively more useful than the other. On the one hand, rich scattering can enable huge resolution gains with finite-sized apertures compared to the LOS-only case. On the other hand, with limited scattering in the environment, even infinite-sized apertures are insufficient to achieve the Rayleigh limit with NLOS-only propagation, unlike the LOS-only case. The drastic difference between the outcomes in both regimes is precisely the reason for the dichotomous conclusions drawn in prior work on multipath, which we survey below.

C. Prior Results on Multipath DoF

Theorem 2 (Multipath DoF [27]–[36]): Let $H_{\text{multi}} = H_{\text{LOS}} + H_{\text{NLOS}}$ denote the operator as per Definition 1 for the multipath Green's function in (5). The sets $\Omega^{(k)}$ and \mathcal{T} are as defined in Theorem 1.

- 1) The operator H_{multi} is compact.
- 2) In the limit of infinite-sized apertures, $m_{eff}(\mathcal{A}) \to \infty$, the achievable DoF d_{img} is

$$\begin{split} &\mathsf{d}_{\mathsf{img}} = \mathsf{dim}\left(\mathsf{col}\left(\mathsf{H}_{\mathsf{multi}}\right)\right) = N_{\mathsf{multi}} + o\left(N_{\mathsf{multi}}\right), \\ &N_{\mathsf{multi}} = \left(\frac{\mathsf{m}\left(\mathcal{T}\right)\mathsf{m}\left(\Omega^{(N+1)}\right)}{\pi}\right) \left(\frac{\mathsf{m}_{\mathsf{eff}}\left(\mathcal{I}\right)2\pi^{N-1}}{\left(2\pi c\right)^{N}\left(N+1\right)}\right), \end{split}$$

assuming the bandwidth Ω has non-zero measure, $\mathsf{m}\left(\Omega\right)>0$. In the special case of single frequency illumination, $\Omega=\{\omega_0\}$,

$$N_{\mathrm{multi}} = \left(\frac{2\mathrm{m}_{\mathrm{eff}}\left(\mathcal{I}\right)2\pi^{N-1}\omega_{0}^{N}}{\left(2\pi c\right)^{N}}\right).$$

3) However, numerical evidence suggests that DoF N_{multi} above is achievable even using finite-sized apertures.

To illustrate the dichotomy between the two conclusions in 2) and 3) in Theorem 2, let us consider Example 2. With $\mathsf{m}_{\mathsf{eff}}(\mathcal{I})$ defined as in (13), $\Omega = [-\omega_0 - \pi W, -\omega_0 + \pi W] \cup [\omega_0 - \pi W, \omega_0 + \pi W]$ and $\mathcal{T} = [0, T]$, for W > 0, we have

$$N_{\mathsf{multi}} = 2WT \cdot \left(\frac{4L_{\mathsf{i}}\cos\theta_{\mathsf{o}}}{\lambda_{\mathsf{0}}}\right),$$
 (27)

where $\lambda_0 = \frac{2\pi c}{\omega_0}$ is the wavelength corresponding to ω_0 . Moreover, the DoF is given by the term in parenthesis above in the special case of W=0, i.e., single frequency illumination.

Therefore, via Definition 5, the spatial resolution δ is

$$\delta = \frac{\lambda_0}{2\cos\theta_0},\tag{28}$$

which corresponds to the Rayleigh limit when $\theta_0 = 0$.

In other words, conclusion 2) in Theorem 2 suggests that given infinite-sized apertures, multipath propagation overcomes the downsides of NLOS-only propagation and achieves the Rayleigh limit, similar to the LOS-only case. This result has led the authors in [16], [27], [28] to conclude that multipath offers no benefits over LOS-only propagation and effectively only shapes the singular values of the Green's function operator.

However, the above drawn conclusion is seemingly at odds with conclusion 3), which states that the Rayleigh limit is achievable even with finite-sized apertures, as per numerical analysis in [29]–[36].

In the next section, we show that conclusions 2) and 3) in fact correspond to two different operating regimes, and remain valid in their respective regimes. We establish this result by deriving the DoF with multipath for practical finite-sized apertures.

V. MAIN RESULTS

We first present the main result of this paper in Theorem 3. We then use the linear aperture and scene example (Example 2) to demonstrate that Theorem 3 unifies the two seemingly disparate conclusions from Theorem 2. Finally, we derive precise conditions under which multipath improves the resolution compared to LOS-only propagation.

A. Main Result

The following theorem characterizes the DoF with multipath in the more general setting with finite-sized apertures.

Theorem 3: With H_{multi} and $\Omega^{(k)}$ defined as in Theorem 2, the DoF with multipath is upper and lower bounded as

$$N_{\ell} + o(N_{\ell}) \le d_{\text{img}} = \dim(\text{col}(H_{\text{multi}})) \le N_{u} + o(N_{u}),$$

where N_{ℓ} and N_u are lower and upper bounds on d_{img} , which are defined in terms of the LOS and NLOS DoFs, N_{LOS} and N_{NLOS} , from Theorem 1,

$$\begin{split} N_{\ell} &= 2\Delta - N_{\mathsf{LOS}} - N_{\mathsf{NLOS}}, \\ N_{u} &= \Delta, \\ \Delta &= \left(\frac{\mathsf{m}\left(\mathcal{T}\right)\mathsf{m}\left(\Omega^{(N+1)}\right)}{\pi}\right) \left(\frac{\min\left\{C,D\right\}}{\left(2\pi c\right)^{N}\left(N+1\right)}\right), \\ C &= \mathsf{m}_{\mathsf{eff}}\left(\mathcal{A}\right)\mathsf{m}\left(\Psi_{\mathsf{ia}} \cup \Psi_{\mathsf{Sa}}\right), \ D &= \mathsf{m}_{\mathsf{eff}}\left(\mathcal{I}\right)\mathsf{m}\left(\Psi_{\mathsf{ai}} \cup \Psi_{\mathsf{si}}\right), \end{split}$$

assuming the bandwidth Ω has non-zero measure, $m(\Omega) > 0$. In the special case of single frequency illumination, $\Omega = \{\omega_0\}$,

$$\Delta = \left(\frac{2\min\left\{C, D\right\}\omega_0^N}{\left(2\pi c\right)^N}\right).$$

Proof: To prove the theorem, we apply the following result from [41] for the sum of two operators, $T = T_1 + T_2$,

$$\begin{split} D_1 + D_2 - D_3 & \leq \dim\left(\operatorname{col}\left(\mathsf{T}\right)\right) \leq \max\left\{D_1, D_2\right\}, \\ D_1 & = \dim\left(\operatorname{col}\left(\mathsf{T}_1\right) + \operatorname{col}\left(\mathsf{T}_2\right)\right), \\ D_2 & = \dim\left(\operatorname{row}\left(\mathsf{T}_1\right) + \operatorname{row}\left(\mathsf{T}_2\right)\right), \\ D_3 & = \dim\left(\operatorname{col}\left(\mathsf{T}_1\right)\right) + \dim\left(\operatorname{col}\left(\mathsf{T}_2\right)\right). \end{split}$$

In the context of our problem, we have $H_{multi} = H_{LOS} + H_{NLOS}$, with $dim\left(col\left(H_{LOS}\right)\right)$ and $dim\left(col\left(H_{NLOS}\right)\right)$ given via Theorem 1. Therefore, it only remains to characterize $dim\left(col\left(H_{LOS}\right) + col\left(H_{NLOS}\right)\right)$ and $dim\left(row\left(H_{LOS}\right) + row\left(H_{NLOS}\right)\right)$ for our model.

To that end, note that with multipath, the transmit and receive spaces $\mathcal X$ and $\mathcal Y$ from (7) and (9) have dimensionalities

$$\begin{split} \dim\left(\mathcal{X}\right) &= \left(\frac{\mathsf{m}\left(\mathcal{T}\right)\mathsf{m}\left(\Omega^{(N+1)}\right)}{\pi}\right) \left(\frac{\mathsf{m}_{\mathsf{eff}}\left(\mathcal{I}\right)\mathsf{m}\left(\Psi_{\mathsf{ai}}\cup\Psi_{\mathsf{si}}\right)}{\left(2\pi c\right)^{N}\left(N+1\right)}\right),\\ \dim\left(\mathcal{Y}\right) &= \left(\frac{\mathsf{m}\left(\mathcal{T}\right)\mathsf{m}\left(\Omega^{(N+1)}\right)}{\pi}\right) \left(\frac{\mathsf{m}_{\mathsf{eff}}\left(\mathcal{A}\right)\mathsf{m}\left(\Psi_{\mathsf{ia}}\cup\Psi_{\mathsf{sa}}\right)}{\left(2\pi c\right)^{N}\left(N+1\right)}\right), \end{split}$$

assuming the bandwidth Ω has non-zero measure, $m\left(\Omega\right)>0$. The dimensionalities for the single frequency illumination case are defined analogously as in Theorem 1. In other words, with multipath, the transmit space $\mathcal X$ corresponds to the product of the effective scene size, $m_{eff}\left(\mathcal I\right)$, and the total angular spread

at the scene, $m(\Psi_{ai} \cup \Psi_{si})$. The receive space \mathcal{Y} is defined analogously from the aperture's perspective.

Therefore, the combined column and row spaces, $col(H_{LOS}) + col(H_{NLOS})$ and $row(H_{LOS}) + row(H_{NLOS})$, are subspaces of dimension

$$\Delta = \min \left\{ \dim \left(\mathcal{X} \right), \dim \left(\mathcal{Y} \right) \right\},$$

corresponding to the minimum of the transmit and receive space dimensionalities, similar to Theorem 1. The desired result follows immediately.

Theorem 3 generalizes conclusion 2) of Theorem 2 from infinite-sized apertures to finite-sized apertures. Moreover, Theorem 3 remains consistent with conclusion 2) of Theorem 2 in the infinite-sized aperture case. To see how, let us substitute $\mathsf{m}_{\mathsf{eff}}(\mathcal{A}) \to \infty$ in Theorem 3,

$$\begin{split} C &= \mathsf{m}_{\mathsf{eff}} \left(\mathcal{A} \right) \mathsf{m} \left(\Psi_{\mathsf{ia}} \cup \Psi_{\mathsf{sa}} \right) = \infty, \\ D &= \mathsf{m}_{\mathsf{eff}} \left(\mathcal{I} \right) \mathsf{m} \left(\Psi_{\mathsf{ai}} \cup \Psi_{\mathsf{si}} \right) = \mathsf{m}_{\mathsf{eff}} \left(\mathcal{I} \right) \mathsf{m} \left(\Psi_{\mathsf{ai}} \right) = \mathsf{m}_{\mathsf{eff}} \left(\mathcal{I} \right) 2 \pi^{N-1} \end{split}$$

where the latter equality for D follows from the fact that the angular interval subtended by aperture onto imaging scene is $\Psi_{\rm ai} = [0,\pi]^N$ for infinite aperture size, for which m $(\Psi_{\rm ai}) = 2\pi^{N-1}$ as per the solid angle measure definition in (10).

Substituting the values of C and D, we thus have

$$N_u = \Delta = N_{\text{multi}},$$
 (29)

which matches the result from Theorem 2. Moreover, note that since $m(\Psi_{ai}) = 2\pi^{N-1}$, we also have $N_{LOS} = \Delta = N_{multi}$. Therefore, the lower bound N_{ℓ} is given by

$$N_{\ell} = \Delta - N_{\text{NLOS}} = N_{\text{multi}} - N_{\text{NLOS}}.$$
 (30)

The gap between the upper and lower bounds is thus $(N_u - N_\ell) = N_{\text{NLOS}}$, which is small for small values of the scene size-NLOS angular interval product, $m_{\text{eff}} \, (\mathcal{I}) \, \text{m} \, (\Psi_{\text{si}})$.

B. Theorem 3 Unifies Conclusions 2) & 3) of Theorem 2

We now use Example 2 to illustrate that Theorem 3 unifies the two seemingly contradictory conclusions of Theorem 2.

To that end, with $\mathsf{m}_{\mathsf{eff}}(\mathcal{A})$, $\mathsf{m}_{\mathsf{eff}}(\mathcal{I})$, $\mathsf{m}\left(\Psi_{\mathsf{ia}}\right)$ and $\mathsf{m}\left(\Psi_{\mathsf{ai}}\right)$ defined as in (12)-(15), $\Omega = \left[-\omega_0 - \pi W, -\omega_0 + \pi W\right] \cup \left[\omega_0 - \pi W, \omega_0 + \pi W\right]$ and $\mathcal{T} = [0, T]$, for W > 0, we have

$$\Delta = 2WT \cdot \left(\frac{2\cos\theta_{\rm o}}{\lambda_0}\min\left\{L_{\rm a}{\rm m}\left(\Psi_{\rm ia}\cup\Psi_{\rm sa}\right),L_{\rm i}{\rm m}\left(\Psi_{\rm ai}\cup\Psi_{\rm si}\right)\right\}\right), \quad (31)$$

where $\lambda_0 = \frac{2\pi c}{\omega_0}$ is the wavelength corresponding to ω_0 . Moreover, the DoF is given by the term in parenthesis above in the special case of W=0, i.e., single frequency illumination.

As before, the effects of bandwidth W, polarization and misorientation angle $\theta_{\rm o}$ on the DoF in (31) remain unchanged compared to the LOS and NLOS cases from (16) and (17). To show that Theorem 3 unifies the results of Theorem 2, let us consider the two regimes used to illustrate all results thus far: (i) infinite-sized apertures, $L_{\rm a} \to \infty$, with limited scattering, m $(\Psi_{\rm sa}) < 2$, m $(\Psi_{\rm si}) < 2$, and (ii) rich scattering with m $(\Psi_{\rm sa}) = {\rm m} (\Psi_{\rm si}) = 2$.

(i) Consider the infinite-sized aperture regime, $L_{\rm a} \to \infty$, with limited scattering in the environment, m $(\Psi_{\rm sa}) < 2$, m $(\Psi_{\rm si}) < 2$. Since we have already shown in (29) that

the upper bound N_u equals N_{multi} from Theorem 2, similar to (28), the spatial resolution δ_u equals the Rayleigh limit,

$$\delta_u = \frac{\lambda_0}{2\cos\theta_0}. (32)$$

On the other hand, consider the lower bound N_{ℓ} , given by (30). In this case, the spatial resolution δ_{ℓ} equals

$$\delta_{\ell} = \frac{\lambda_0}{2\cos\theta_o} \cdot \frac{1}{1 - \frac{\mathsf{m}(\Psi_{si})}{2}},\tag{33}$$

which is close to the Rayleigh limit for small m (Ψ_{si}).

Compare (32) and (33) to (26) for NLOS-only propagation. Both δ_ℓ and δ_u are close to the Rayleigh limit, especially when $m(\Psi_{si})$ is small, i.e., scattering is limited in the environment. By contrast, the opposite holds for NLOS-only propagation, where the Rayleigh limit is never achievable with limited scattering. Thus, multipath overcomes the downsides of NLOS-only propagation and is effectively equivalent to LOS-only propagation with limited scattering, consistent with conclusion 2) of Theorem 2.

(ii) Consider the rich scattering regime with $m(\Psi_{sa}) = m(\Psi_{si}) = 2$. In this case, we had shown earlier that with NLOS-only propagation, the Rayleigh limit is achievable using finite aperture sizes, $L_a = L_i$. By contrast, achieving the Rayleigh limit requires infinite-sized apertures in LOS case.

For multipath, the value of Δ matches N_{NLOS} from (17),

$$\Delta = N_u = N_{\text{NLOS}} = 2WT \cdot \left(\frac{4\cos\theta_{\text{o}}}{\lambda_0}\min\{L_{\text{a}}, L_{\text{i}}\}\right). (34)$$

Thus, the resolution δ_u corresponding to the upper bound N_u matches the resolution δ from (24) for the NLOS case. Hence, the Rayleigh limit is achieved using finite aperture sizes, $L_{\rm a}=L_{\rm i}$, in this case as well.

Furthermore, the lower bound N_{ℓ} in Theorem 3 equals

$$N_{\ell} = 2\Delta - N_{LOS} - N_{NLOS} = \Delta - N_{LOS}. \tag{35}$$

Thus, the resolution δ_{ℓ} corresponding to N_{ℓ} is

$$\delta_{\ell} = \frac{\lambda_0}{2\cos\theta_{o}} \cdot \frac{L_{i}}{\min\left\{L_{a}, L_{i}\right\} - L_{i}\sin\left(\tan^{-1}\left(\frac{L_{a}}{2D}\right)\right)}. \quad (36)$$

The resolution δ_ℓ is minimized when the denominator $\min\{L_{\mathsf{a}},L_{\mathsf{i}}\}-L_{\mathsf{i}}\sin\left(\tan^{-1}\left(\frac{L_{\mathsf{a}}}{2D}\right)\right)$ is maximum, i.e., at $L_{\mathsf{a}}=L_{\mathsf{i}}$. For $L_{\mathsf{a}}=L_{\mathsf{i}}$, the minimum achievable resolution equals

$$\delta_{\ell} = \frac{\lambda_0}{2\cos\theta_{o}} \cdot \frac{1}{1 - \sin\left(\tan^{-1}\left(\frac{L_{i}}{2D}\right)\right)},\tag{37}$$

which is close to the Rayleigh limit for small values of L_i .

In other words, given rich scattering, the resolution corresponding to both multipath DoF bounds in Theorem 3 is minimized, and is close to the Rayleigh limit, at *finite* aperture sizes, $L_{\rm a}=L_{\rm i}$, similar to the NLOS-only case. We illustrate this result in Fig. 8, where we plot the normalized resolution, $\frac{\delta_\ell}{\left(\frac{\lambda_0}{2\cos\theta_0}\right)}$ and $\frac{\delta_u}{\left(\frac{\lambda_0}{2\cos\theta_0}\right)}$, for the same example from Fig. 7. Hence, multipath propagation is effectively equivalent to, and captures the gains of, NLOS-only propagation in the rich scattering regime. Furthermore, rich scattering enables drastic resolution gains over LOS-only propagation, as predicted by conclusion 3) of Theorem 2.

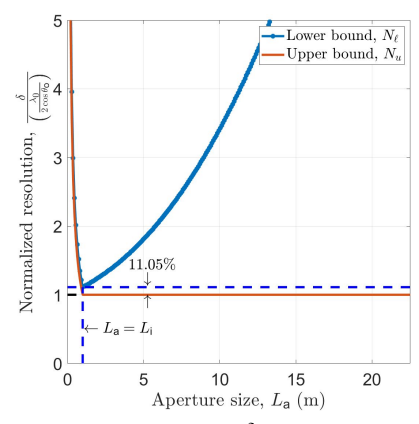


Fig. 8: Normalized resolution $\frac{\delta}{\left(\frac{\lambda_0}{2\cos\theta_o}\right)}$ vs aperture size L_a for multipath propagation in a rich scattering indoor environment. System parameters are as in Fig. 7. Resolution is minimized at $L_a = L_i = 1$ m, similar to NLOS-only case from Fig. 7, and is within $\frac{\sin\left(\tan^{-1}\left(\frac{L_i}{2D}\right)\right)}{1-\sin\left(\tan^{-1}\left(\frac{L_i}{2D}\right)\right)} = 11.05\%$ error of Rayleigh limit. \therefore multipath \equiv NLOS-only propagation in this regime.

From the discussion in cases (i) and (ii) above, we see that both sets of conclusions in Theorem 2 are valid in their respective regimes. Our main result thus unifies both conclusions of Theorem 2. Moreover, cases (i) and (ii) illustrate that multipath effectively captures the best of both worlds and compensates for the weaknesses of both LOS-only and NLOS-only propagation in respective regimes.

Having established that Theorem 3 unifies both sets of conclusions from Theorem 2, we now derive conditions under which multipath improves the resolution compared to LOS-only propagation.

C. When Does Multipath Improve Resolution Beyond LOS?

We begin by comparing the upper and lower DoF bounds from Theorem 3 with the LOS DoF from Theorem 1.

Observation 1: The upper bound $N_u = \Delta$ from Theorem 3 always exceeds LOS DoF N_{LOS} from Theorem 1 since the angular intervals always satisfy the property

$$\mathsf{m}\left(\Psi_{\mathsf{ia}} \cup \Psi_{\mathsf{sa}}\right) \geq \mathsf{m}\left(\Psi_{\mathsf{ia}}\right), \ \mathsf{m}\left(\Psi_{\mathsf{ai}} \cup \Psi_{\mathsf{si}}\right) \geq \mathsf{m}\left(\Psi_{\mathsf{ai}}\right).$$

Observation 2: The lower bound $N_\ell=2\Delta-N_{\rm LOS}-N_{\rm NLOS}$ from Theorem 3 exceeds LOS DoF $N_{\rm LOS}$ from Theorem 1 if

$$2\left(\Delta - N_{\mathsf{LOS}}\right) = 2\left(N_u - N_{\mathsf{LOS}}\right) \ge N_{\mathsf{NLOS}},\tag{38}$$

which is also a sufficient condition for $N_{\text{multi}} \geq N_{\text{LOS}}$.

To gain some intuition for (38), let us consider Example 2. With N_{LOS} , N_{NLOS} and Δ as given in (16), (17) and (31), we may express (38) as

$$2\min\left\{L_{\mathsf{a}}\mathsf{m}\left(\Psi_{\mathsf{sa}}\setminus\Psi_{\mathsf{ia}}\right),L_{\mathsf{i}}\mathsf{m}\left(\Psi_{\mathsf{si}}\setminus\Psi_{\mathsf{ai}}\right)\right\}\geq\min\left\{L_{\mathsf{a}}\mathsf{m}\left(\Psi_{\mathsf{sa}}\right),L_{\mathsf{i}}\mathsf{m}\left(\Psi_{\mathsf{si}}\right)\right\},\quad \ \left(39\right)$$

or, on using the identity $m(A \setminus B) = m(A) - m(A \cap B)$, as

$$L_{\mathsf{a}}\mathsf{m}\left(\Psi_{\mathsf{s}\mathsf{a}}\right) - 2L_{\mathsf{a}}\mathsf{m}\left(\Psi_{\mathsf{s}\mathsf{a}}\cap\Psi_{\mathsf{i}\mathsf{a}}\right) + \left[L_{\mathsf{a}}\mathsf{m}\left(\Psi_{\mathsf{s}\mathsf{a}}\right) - L_{\mathsf{i}}\mathsf{m}\left(\Psi_{\mathsf{s}\mathsf{i}}\right)\right]^{+} \ge 0, \quad (40)$$

$$L_{\mathrm{i}}\mathrm{m}\left(\Psi_{\mathrm{si}}\right)-2L_{\mathrm{i}}\mathrm{m}\left(\Psi_{\mathrm{si}}\cap\Psi_{\mathrm{ai}}\right)+\left[L_{\mathrm{i}}\mathrm{m}\left(\Psi_{\mathrm{si}}\right)-L_{\mathrm{a}}\mathrm{m}\left(\Psi_{\mathrm{sa}}\right)\right]^{+}\geq0,\ \ (41)$$

where $[\cdot]^+$ denotes the positive part.

To better understand (40) and (41), let us consider the two regimes used to illustrate all results thus far: (i) rich scattering with $m\left(\Psi_{\mathsf{sa}}\right) = m\left(\Psi_{\mathsf{si}}\right) = 2$, and (ii) infinite-sized apertures, $L_{\mathsf{a}} \to \infty$, with limited scattering, $m\left(\Psi_{\mathsf{sa}}\right) < 2$, $m\left(\Psi_{\mathsf{si}}\right) < 2$.

(i) In the rich scattering regime, we have $\Psi_{\mathsf{sa}} \cap \Psi_{\mathsf{ia}} = \Psi_{\mathsf{ia}}$ and $\Psi_{\mathsf{si}} \cap \Psi_{\mathsf{ai}} = \Psi_{\mathsf{ai}}$. Thus, (40) and (41) are equivalent to

$$2L_{a} - 2L_{a} m (\Psi_{ia}) + 2[L_{a} - L_{i}]^{+} \ge 0,$$
 (42)

$$2L_{i} - 2L_{i}m(\Psi_{ai}) + 2[L_{i} - L_{a}]^{+} \ge 0,$$
 (43)

both of which are satisfied by default, since the left hand sides are always greater than zero. Moreover, both left hand sides are simultaneously maximized when $L_{\rm i}=L_{\rm a}$, consistent with our previous analysis and Fig. 8. Thus, multipath outperforms LOS-only propagation in the rich scattering regime with practical finite-sized apertures.

(ii) In the limited scattering regime with infinite-sized apertures, we have $\Psi_{si} \cap \Psi_{ai} = \Psi_{si}$. Moreover, we only need to consider (41) since $L_a \to \infty$ invalidates (40). To that end, note that the left hand side of (41) equals

$$-L_{\mathsf{i}}\mathsf{m}\left(\Psi_{\mathsf{s}\mathsf{i}}\right)+\left[L_{\mathsf{i}}\mathsf{m}\left(\Psi_{\mathsf{s}\mathsf{i}}\right)-L_{\mathsf{a}}\mathsf{m}\left(\Psi_{\mathsf{s}\mathsf{a}}\right)\right]^{+},$$

which is always less than zero, with equality only when $m(\Psi_{si}) = 0$, i.e., LOS-only propagation. Hence, multipath performs similar to LOS-only propagation in the limited scattering regime, consistent with our earlier analysis.

To summarize, multipath can indeed improve the resolution beyond LOS-only propagation when the condition in (38) is satisfied. Since (38) is satisfied for finite apertures in the rich scattering regime, consistent with conclusion 3) of Theorem 2, we observe that multipath significantly outperforms LOS in this regime. In fact, as demonstrated earlier, multipath achieves the Rayleigh limit when the aperture and scene extents are equal, $L_i = L_a$. By contrast, LOS-only propagation is insufficient to achieve the Rayleigh limit with finite-sized apertures.

On the other hand, (38) is not satisfied for infinite-sized apertures. Hence, multipath is at best equivalent to LOS-only propagation in this regime, consistent with conclusion 2) of Theorem 2.

Overall, our results highlight the benefits of harnessing multipath for imaging. As we have shown, multipath is especially beneficial in the rich scattering regime with practical finite-sized apertures. Although all the results in this section were derived for single-bounce scattering modeled via (6), we show in Appendix A that the extension to multiple bounces (all the way up to infinite bounces) does not change our main results.

VI. CONCLUDING REMARKS

In this paper, we characterized the resolution limits for wireless imaging systems in the presence of multipath via the DoF framework. Via the DoF analysis, we bridged the gap between two sets of prior results, that respectively claimed that multipath does and does not improve resolution beyond LOS-only propagation. We showed that the two sets of prior results correspond to two extreme operational regimes, and that both results are valid in respective regimes. We also showed that multipath can indeed improve the resolution beyond LOS-only propagation under certain geometrical configurations of scatterers in the environment.

Taken together, our results highlight the benefits of harnessing multipath in emerging wireless imaging systems. We hope that the encouraging theoretical results presented in this paper will motivate further research on practical algorithms and system designs that harness the resolution gains provided by multipath.

As all our results were limited to passive illumination with no mobility, extensions to the active illumination setting with mobility would be useful. Extending our deterministic results to the mobility setting is non-trivial since mobility induces an element of randomness in the propagation characteristics. In this context, it would be useful to consider recently proposed hybrid representations [25], [42], [43] that capture the best of both statistical and deterministic channel models. To our knowledge, DoF and resolution limits using such hybrid representations have remained limited to LOS-only propagation thus far, with the exception of [44].

APPENDIX A

EXTENSION OF (1) TO MULTI-BOUNCE SCATTERING

We start by extending the NLOS Green's function in (6) to model double-bounce scattering before presenting the extension to infinite bounces. Throughout, we use the superscript $(\cdot)^{(n)}$ to denote the *n*th bounce term, $\forall n \geq 2$, and $(\cdot)^{(1:k)}$ to denote the sum of first k bounces, $\forall k \geq 2$.

The second-bounce term is given by

$$\mathbf{H}_{\mathrm{NLOS}}^{(2)}\left(\mathbf{r}_{\mathrm{a}},\mathbf{r}_{\mathrm{i}};\omega\right)=\int_{\mathcal{S}}\int_{\mathcal{S}}\mathbf{H}_{\mathrm{LOS}}\left(\mathbf{r}_{\mathrm{a}},\mathbf{r}_{\mathrm{s}}';\omega\right)\cdot\mathrm{diag}\left(\mathbf{h}\left(\mathbf{r}_{\mathrm{s}}';\omega\right)\right)\cdot$$

 $\mathbf{H}_{\mathsf{LOS}}(\mathbf{r}_{\mathsf{s}}', \mathbf{r}_{\mathsf{s}}; \omega) \cdot \mathsf{diag}(\mathbf{h}(\mathbf{r}_{\mathsf{s}}; \omega)) \cdot \mathbf{H}_{\mathsf{LOS}}(\mathbf{r}_{\mathsf{s}}, \mathbf{r}_{\mathsf{i}}; \omega) \, \mathsf{d}\mathbf{r}_{\mathsf{s}} \mathsf{d}\mathbf{r}_{\mathsf{s}}', \quad (44)$

which may be decomposed in two ways:

1)
$$\mathbf{H}_{\mathsf{NLOS}}^{(2)}(\mathbf{r}_{\mathsf{a}}, \mathbf{r}_{\mathsf{i}}; \omega) = \int_{\mathcal{S}} \mathbf{H}_{\mathsf{LOS}}(\mathbf{r}_{\mathsf{a}}, \mathbf{r}_{\mathsf{s}}; \omega) \cdot \mathsf{diag}(\mathbf{h}(\mathbf{r}_{\mathsf{s}}; \omega)) \cdot \mathbf{H}_{\mathsf{LOS}}^{(2)}(\mathbf{r}_{\mathsf{s}}, \mathbf{r}_{\mathsf{i}}; \omega) \, \mathsf{dr}_{\mathsf{s}}, \quad \text{where} \quad \mathbf{H}_{\mathsf{LOS}}^{(2)}(\mathbf{r}_{\mathsf{s}}, \mathbf{r}_{\mathsf{i}}; \omega) = \int_{\mathcal{S}} \mathbf{H}_{\mathsf{LOS}}(\mathbf{r}_{\mathsf{s}}, \mathbf{r}_{\mathsf{i}}'; \omega) \cdot \mathsf{diag}(\mathbf{h}(\mathbf{r}_{\mathsf{s}}'; \omega)) \cdot \mathbf{H}_{\mathsf{LOS}}(\mathbf{r}_{\mathsf{s}}', \mathbf{r}_{\mathsf{i}}; \omega) \, \mathsf{dr}_{\mathsf{s}}'.$$

1)
$$\mathbf{H}_{\text{NLOS}}^{(2)}(\mathbf{r}_{\mathsf{a}}, \mathbf{r}_{\mathsf{i}}; \omega) = \int_{\mathcal{S}} \mathbf{H}_{\text{LOS}}(\mathbf{r}_{\mathsf{a}}, \mathbf{r}_{\mathsf{s}}; \omega) \cdot \text{diag}(\mathbf{h}(\mathbf{r}_{\mathsf{s}}; \omega)) \cdot \mathbf{H}_{\text{LOS}}^{(2)}(\mathbf{r}_{\mathsf{s}}, \mathbf{r}_{\mathsf{i}}; \omega) \, d\mathbf{r}_{\mathsf{s}}, \quad \text{where} \quad \mathbf{H}_{\text{LOS}}^{(2)}(\mathbf{r}_{\mathsf{s}}, \mathbf{r}_{\mathsf{i}}; \omega) = \int_{\mathcal{S}} \mathbf{H}_{\text{LOS}}(\mathbf{r}_{\mathsf{s}}, \mathbf{r}_{\mathsf{i}}; \omega) \cdot \text{diag}(\mathbf{h}(\mathbf{r}_{\mathsf{s}}'; \omega)) \cdot \mathbf{H}_{\text{LOS}}(\mathbf{r}_{\mathsf{s}}', \mathbf{r}_{\mathsf{i}}; \omega) \, d\mathbf{r}_{\mathsf{s}}', \\ 2) \quad \mathbf{H}_{\text{NLOS}}^{(2)}(\mathbf{r}_{\mathsf{a}}, \mathbf{r}_{\mathsf{i}}; \omega) = \int_{\mathcal{S}} \mathbf{H}_{\text{LOS}}^{(2)}(\mathbf{r}_{\mathsf{a}}, \mathbf{r}_{\mathsf{s}}; \omega) \cdot \text{diag}(\mathbf{h}(\mathbf{r}_{\mathsf{s}}; \omega)) \cdot \mathbf{H}_{\text{LOS}}(\mathbf{r}_{\mathsf{s}}', \mathbf{r}_{\mathsf{s}}; \omega) = \int_{\mathcal{S}} \mathbf{H}_{\text{LOS}}(\mathbf{r}_{\mathsf{a}}, \mathbf{r}_{\mathsf{s}}'; \omega) \cdot \text{diag}(\mathbf{h}(\mathbf{r}_{\mathsf{s}}'; \omega)) \cdot \mathbf{H}_{\text{LOS}}(\mathbf{r}_{\mathsf{s}}', \mathbf{r}_{\mathsf{s}}; \omega) \, d\mathbf{r}_{\mathsf{s}}'.$$
The first decomposition above corresponds to modeling

The first decomposition above corresponds to modeling double-bounce in the radiation from the imaging scene to the set of scatterers. On the other hand, the second decomposition corresponds to modeling double-bounce in the reception at the aperture from the scatterers.

Let the operators H_i and H_a denote the transformations from $\mathbf{H}_{\mathsf{LOS}}(\mathbf{r}_{\mathsf{s}},\mathbf{r}_{\mathsf{i}};\omega)$ to $\mathbf{H}_{\mathsf{LOS}}^{(2)}(\mathbf{r}_{\mathsf{s}},\mathbf{r}_{\mathsf{i}};\omega)$ and from $\mathbf{H}_{\mathsf{LOS}}(\mathbf{r}_{\mathsf{a}},\mathbf{r}_{\mathsf{s}};\omega)$ to $\mathbf{H}_{LOS}^{(2)}(\mathbf{r}_{a},\mathbf{r}_{s};\omega)$ respectively,

$$\mathbf{H}_{LOS}^{(2)}(\mathbf{r}_{s}, \mathbf{r}_{i}; \omega) = \mathsf{H}_{i}(\mathbf{H}_{LOS}(\mathbf{r}_{s}, \mathbf{r}_{i}; \omega)), \qquad (45)$$

$$\mathbf{H}_{\mathsf{LOS}}^{(2)}\left(\mathbf{r}_{\mathsf{a}},\mathbf{r}_{\mathsf{s}};\omega\right)=\mathsf{H}_{\mathsf{a}}\left(\mathbf{H}_{\mathsf{LOS}}\left(\mathbf{r}_{\mathsf{a}},\mathbf{r}_{\mathsf{s}};\omega\right)\right). \tag{46}$$

Then, the infinite-bounce extensions of $\mathbf{H}_{LOS}(\mathbf{r}_{s}, \mathbf{r}_{i}; \omega)$ and $\mathbf{H}_{\mathsf{LOS}}\left(\mathbf{r}_{\mathsf{a}},\mathbf{r}_{\mathsf{s}};\omega\right)$ are given by the Neumann series,

$$\mathbf{H}_{\mathsf{LOS}}^{(1:\infty)}\left(\mathbf{r}_{\mathsf{s}}, \mathbf{r}_{\mathsf{i}}; \omega\right) = \left(\sum_{k=0}^{\infty} \mathsf{H}_{\mathsf{i}}^{k}\right) \left(\mathbf{H}_{\mathsf{LOS}}\left(\mathbf{r}_{\mathsf{s}}, \mathbf{r}_{\mathsf{i}}; \omega\right)\right), \quad (47)$$

$$\mathbf{H}_{\mathsf{LOS}}^{(1:\infty)}\left(\mathbf{r}_{\mathsf{a}}, \mathbf{r}_{\mathsf{s}}; \omega\right) = \left(\sum_{k=0}^{\infty} \mathsf{H}_{\mathsf{a}}^{k}\right) \left(\mathbf{H}_{\mathsf{LOS}}\left(\mathbf{r}_{\mathsf{a}}, \mathbf{r}_{\mathsf{s}}; \omega\right)\right), \quad (48)$$

where $\mathsf{T}^k = \mathsf{T}^{k-1} \circ \mathsf{T}$ denotes the kth repeated application of an operator T. Moreover, the Neumann series converge to the invertible operator $\sum_{k=0}^{\infty} \mathsf{H}_{j}^{k} = (\mathsf{I} - \mathsf{H}_{j})^{-1}, \ \forall j \in \{\mathsf{i}, \mathsf{a}\}, \text{ for } \mathsf{h}_{j}^{k} = \mathsf{I}_{j}^{k}$ identity operator I, when operators H_i and H_a have norm < 1. This convergence always holds physically due to conservation of energy and the impossibility of infinite-energy fields.

We are now ready to show that the infinite-bounce extensions in (47) and (48) do not change our main result from Theorem 3. Let $H_{NLOS,i}^{(1:\infty)}$ and $H_{NLOS,a}^{(1:\infty)}$ be the infinitebounce analogues of the NLOS operator H_{NLOS}, defined as in Definition 1, corresponding to (47) and (48). Note that by definition, (47) only affects the row space of H_{NLOS} while (48) only affects the column space of H_{NLOS}.

However, since the Neumann series converge to invertible operators in (47) and (48), we must have

$$row\left(\mathsf{H}_{\mathsf{NLOS},\mathsf{i}}^{(1:\infty)}\right) = row\left(\mathsf{H}_{\mathsf{NLOS}}\right),\tag{49}$$

$$\operatorname{row}\left(\mathsf{H}_{\mathsf{NLOS},\mathsf{i}}^{(1:\infty)}\right) = \operatorname{row}\left(\mathsf{H}_{\mathsf{NLOS}}\right),\tag{49}$$

$$\operatorname{col}\left(\mathsf{H}_{\mathsf{NLOS},\mathsf{i}}^{(1:\infty)}\right) = \operatorname{col}\left(\mathsf{H}_{\mathsf{NLOS}}\right).\tag{50}$$

Thus, since the row and column spaces of H_{NLOS} , and hence their dimensionalities, remain unchanged with infinite-bounce scattering, our main result from Theorem 3 does not change.

REFERENCES

- [1] N. Mehrotra and A. Sabharwal, "DoF Analysis for Multipath-Assisted Imaging: Single Frequency Illumination," in 2020 IEEE International Symposium on Information Theory (ISIT), 2020, pp. 1456-1461.
- N. Mehrotra, "Degrees of Freedom Analysis for Multipath-Assisted Imaging Systems," Master's thesis, Rice University, Nov 2020. [Online]. Available: https://scholarship.rice.edu/handle/1911/109578
- [3] F. Adib and D. Katabi, "See through Walls with WiFi!" in Proceedings of the ACM SIGCOMM 2013 Conference on SIGCOMM, ser. SIGCOMM '13, 2013, p. 75-86.
- D. Huang, R. Nandakumar, and S. Gollakota, "Feasibility and Limits of Wi-Fi Imaging," in Proceedings of the 12th ACM Conference on Embedded Network Sensor Systems, ser. SenSys '14, 2014, p. 266-279.
- [5] Y. Zhu, Y. Zhu, B. Y. Zhao, and H. Zheng, "Reusing 60GHz Radios for Mobile Radar Imaging," in Proceedings of the 21st Annual International Conference on Mobile Computing and Networking, ser. MobiCom '15. New York, NY, USA: Association for Computing Machinery, 2015, p. 103-116. [Online]. Available: https://doi.org/10.1145/2789168.2790112
- [6] P. M. Holl and F. Reinhard, "Holography of Wi-fi Radiation," Phys. Rev. Lett., vol. 118, p. 183901, May 2017.
- [7] C. R. Karanam and Y. Mostofi, "3D Through-Wall Imaging with Unmanned Aerial Vehicles Using WiFi," in 2017 16th ACM/IEEE International Conference on Information Processing in Sensor Networks (IPSN), 2017, pp. 131-142.
- [8] A. Pedross-Engel, D. Arnitz, J. N. Gollub, O. Yurduseven, K. P. Trofatter, M. F. Imani, T. Sleasman, M. Boyarsky, X. Fu, D. L. Marks, D. R. Smith, and M. S. Reynolds, "Orthogonal Coded Active Illumination for Millimeter Wave, Massive-MIMO Computational Imaging With Metasurface Antennas," IEEE Transactions on Computational Imaging, vol. 4, no. 2, pp. 184-193, 2018.
- S. Vakalis, L. Gong, and J. A. Nanzer, "Imaging With WiFi," IEEE Access, vol. 7, pp. 28616-28624, 2019.
- J. Guan, A. Paidimarri, A. Valdes-Garcia, and B. Sadhu, "3-D Imaging Using Millimeter-Wave 5G Signal Reflections," IEEE Transactions on Microwave Theory and Techniques, vol. 69, no. 6, pp. 2936-2948, 2021.
- [11] G. G. di Francia, "Degrees of Freedom of an Image," Journal of the Optical Society of America, vol. 59, no. 7, pp. 799 – 804, July 1969.
- F. Gori and G. Guattari, "Shannon Number and Degrees of Freedom of an Image," Optics Communications, vol. 7, no. 2, pp. 163 - 165, February 1973.
- [13] R. Piestun and D. A. B. Miller, "Electromagnetic degrees of freedom of an optical system," Journal of the Optical Society of America A, vol. 17, no. 5, p. 892, May 2000.

- [14] F. M. Dickey, L. A. Romero, J. M. DeLaurentis, and A. W. Doerry, "Super-resolution, degrees of freedom and synthetic aperture radar," *IEE Proceedings - Radar, Sonar and Navigation*, vol. 150, no. 6, pp. 419–429, Dec 2003.
- [15] B. Mamandipoor, A. Arbabian, and U. Madhow, "Geometry-constrained Degrees of Freedom Analysis for Imaging Systems: Monostatic and Multistatic," arXiv: Information Theory, Nov 2017. [Online]. Available: http://arxiv.org/abs/1711.03585
- [16] M. Franceschetti, Wave Theory of Information. Cambridge University Press, Nov 2017.
- [17] D. A. B. Miller, "Waves, modes, communications, and optics: a tutorial," Adv. Opt. Photon., vol. 11, no. 3, pp. 679–825, Sep 2019.
- [18] N. Mehrotra and A. Sabharwal, "Simultaneous Imaging & Uplink Communication: A Degrees of Freedom Perspective," in 2021 55th Asilomar Conference on Signals, Systems, and Computers, 2021, pp. 762–766.
- [19] N. Mehrotra and A. Sabharwal, "On the Degrees of Freedom Region for Simultaneous Imaging & Uplink Communication," *IEEE Journal on Selected Areas in Communications*, pp. 1–1, 2022.
- [20] O. Bucci and G. Franceschetti, "On the spatial bandwidth of scattered fields," *IEEE Transactions on Antennas and Propagation*, vol. 35, no. 12, pp. 1445–1455, December 1987.
- [21] O. M. Bucci and G. Franceschetti, "On the degrees of freedom of scattered fields," *IEEE Transactions on Antennas and Propagation*, vol. 37, no. 7, pp. 918–926, July 1989.
- [22] A. S. Y. Poon, R. W. Brodersen, and D. N. C. Tse, "Degrees of freedom in multiple-antenna channels: a signal space approach," *IEEE Transactions on Information Theory*, vol. 51, no. 2, pp. 523–536, Feb 2005
- [23] M. Franceschetti, "On Landau's Eigenvalue Theorem and Information Cut-Sets," *IEEE Transactions on Information Theory*, vol. 61, no. 9, pp. 5042–5051, Sep. 2015.
- [24] A. S. Y. Poon, D. N. C. Tse, and R. W. Brodersen, "Impact of scattering on the capacity, diversity, and propagation range of multiple-antenna channels," *IEEE Transactions on Information Theory*, vol. 52, no. 3, pp. 1087–1100, March 2006.
- [25] A. Pizzo, T. L. Marzetta, and L. Sanguinetti, "Degrees of Freedom of Holographic MIMO Channels," in 2020 IEEE 21st International Workshop on Signal Processing Advances in Wireless Communications (SPAWC), 2020, pp. 1–5.
- [26] A. Pizzo, A. d. J. Torres, L. Sanguinetti, and T. L. Marzetta, "Nyquist-Sampling and Degrees of Freedom of Electromagnetic Fields," arXiv preprint arXiv:2109.10040, 2021.
- [27] R. Janaswamy, "On the EM Degrees of Freedom in Scattering Environments," *IEEE Transactions on Antennas and Propagation*, vol. 59, no. 10, pp. 3872–3881, Oct 2011.
- [28] M. Franceschetti, M. D. Migliore, P. Minero, and F. Schettino, "The Information Carried by Scattered Waves: Near-Field and Nonasymptotic Regimes," *IEEE Transactions on Antennas and Propagation*, vol. 63, no. 7, pp. 3144–3157, July 2015.
- [29] M. Cheney and R. J. Bonneau, "Imaging that exploits multipath scattering from point scatterers," in SPIE 5808, Algorithms for Synthetic Aperture Radar Imagery XII, E. G. Zelnio and F. D. Garber, Eds., vol. 5808. International Society for Optics and Photonics, May 2005, p. 142
- [30] C. J. Nolan, M. Cheney, T. Dowling, and R. Gaburro, "Enhanced angular resolution from multiply scattered waves," *Inverse Problems*, vol. 22, no. 5, pp. 1817–1834, Sep 2006.
- [31] J. Xu and R. Janaswamy, "Electromagnetic Degrees of Freedom in 2-D Scattering Environments," *IEEE Transactions on Antennas and Propagation*, vol. 54, no. 12, pp. 3882–3894, Dec 2006.
- [32] V. Krishnan and B. Yazici, "Synthetic aperture radar imaging exploiting multiple scattering," *Inverse Problems*, vol. 27, no. 5, p. 055004, Mar 2011
- [33] G. Gennarelli and F. Soldovieri, "A Linear Inverse Scattering Algorithm for Radar Imaging in Multipath Environments," *IEEE Geoscience and Remote Sensing Letters*, vol. 10, no. 5, pp. 1085–1089, Sep 2013.
- [34] M. Leigsnering, F. Ahmad, M. G. Amin, and A. M. Zoubir, "Compressive sensing based specular multipath exploitation for through-the-wall radar imaging," in 2013 IEEE International Conference on Acoustics, Speech and Signal Processing, May 2013, pp. 6004–6008.
- [35] M. Leigsnering, M. Amin, F. Ahmad, and A. M. Zoubir, "Multipath Exploitation and Suppression for SAR Imaging of Building Interiors: An overview of recent advances," *IEEE Signal Processing Magazine*, vol. 31, no. 4, pp. 110–119, July 2014.
- [36] R. Solimene, I. Catapano, G. Gennarelli, A. Cuccaro, A. Dell'Aversano, and F. Soldovieri, "SAR Imaging Algorithms and Some Unconventional

- Applications: A unified mathematical overview," *IEEE Signal Processing Magazine*, vol. 31, no. 4, pp. 90–98, July 2014.
- [37] D. Tse and P. Viswanath, Fundamentals of Wireless Communication. Cambridge University Press, 2005.
- [38] E. Everett and A. Sabharwal, "Spatial degrees-of-freedom in large-array full-duplex: the impact of backscattering," EURASIP Journal on Wireless Communications and Networking, vol. 2016, no. 1, pp. 1–23, 2016.
- [39] A. Pinkus, n-widths in Approximation Theory. New York, NY, USA: Springer-Verlag, 1985.
- [40] A. S. Y. Poon and D. N. C. Tse, "Degree-of-Freedom Gain From Using Polarimetric Antenna Elements," *IEEE Transactions on Information Theory*, vol. 57, no. 9, pp. 5695–5709, 2011.
- [41] G. Marsaglia and G. P. H. Styan, "Equalities and Inequalities for Ranks of Matrices," *Linear and Multilinear Algebra*, vol. 2, no. 3, pp. 269–292, 1974. [Online]. Available: https://doi.org/10.1080/03081087408817070
- [42] A. Pizzo, T. Marzetta, and L. Sanguinetti, "Holographic MIMO Communications Under Spatially-Stationary Scattering," arXiv: Information Theory, 2020.
- [43] A. Pizzo, T. L. Marzetta, and L. Sanguinetti, "Spatially-Stationary Model for Holographic MIMO Small-Scale Fading," *IEEE Journal on Selected Areas in Communications*, vol. 38, no. 9, pp. 1964–1979, 2020.
- [44] A. Pizzo, L. Sanguinetti, and T. L. Marzetta, "Spatial Characterization of Electromagnetic Random Channels," arXiv preprint arXiv:2103.15666, 2021



Nishant Mehrotra received the B.Tech. degree (with honors) in Electronics and Electrical Communication Engineering from the Indian Institute of Technology, Kharagpur, India in 2018 and the M.S. degree in Electrical and Computer Engineering from Rice University, Houston, TX, USA in 2020. He is currently pursuing the Ph.D. degree in Electrical and Computer Engineering at Rice University, Houston, TX, USA. His research interests include information theory, joint sensing-communication, and wireless systems.



Ashutosh Sabharwal received the B.Tech. degree from IIT Delhi, New Delhi, India, in 1993, and the M.S. and Ph.D. degrees from The Ohio State University, Columbus, OH, USA, in 1995 and 1999, respectively. He is currently the Department Chair and Ernest D. Butcher Professor at the Department of Electrical and Computer Engineering, Rice University, Houston, TX, USA. His research interests are in wireless theory, design, and large-scale deployed testbeds. He is the founder of the WARP project (warp.rice.edu), an open-source project which is now

in use at more than 125 research groups worldwide and has been used by more than 500 research articles. He is currently leading several NSF-funded center-scale projects, notably Rice RENEW (renew-wireless.org), to develop an open-source software-defined wireless network platform. He received the 2017 IEEE Jack Neubauer Memorial Award, 2018 IEEE Advances in Communications Award, 2019 ACM MobiCom Community Contribution Award, and the 2019 and 2021 ACM Test-of-time Awards. He is a Fellow of IEEE and the National Academy of Inventors.